이학석사 학위논문

$LiTaO_3$ 또는 InF_3의 혼합에 의한 전고체전지용 고체 전해질 $Li_{5.3}PS_{4.3}Cl_{1.7}$의 계면 안정성 향상에 관한 연구

Study on improving the interfacial stability of solid electrolyte $Li_{5.3}PS_{4.3}Cl_{1.7}$ for all-solid-state batteries by mixing $LiTaO_3$ or InF_3

울 산 대 학 교 대 학 원

화 학 과

김 규 식

$LiTaO_3$ 또는 InF_3의 혼합에 의한 전고체전지용 고체 전해질 $Li_{5.3}PS_{4.3}Cl_{1.7}$의 계면 안정성 향상에 관한 연구

Study on improving the interfacial stability of solid electrolyte $Li_{5.3}PS_{4.3}Cl_{1.7}$ for all-solid-state batteries by mixing $LiTaO_3$ or InF_3

지 도 교 수　류 광 선

이 논문을 이학 석사 학위 논문으로 제출함

2023년 12월

울 산 대 학 교 대 학 원

화 학 과

김 규 식

김규식의 이학석사 학위 논문을 인준함

위원장 정 재 훈 印

위 원 정 지 원 印

위 원 류 광 선 印

울 산 대 학 교 대 학 원

2023년 12월

Abstract

Today, all-solid-state batteries(ASSBs) with solid electrolytes(SEs) are receiving a lot of attention as next-generation batteries. Solid electrolytes are chemically more stable than liquid electrolytes, can have higher energy densities, and can operate over a wide temperature range. In particular, sulfide-based solids electrolytes have the advantage of having good mechanical properties and high ionic conductivity, but they have the problem that unwanted side reactions may occur at the interface between the solid electrolyte and the electrode, which may deteriorate battery performance.

In this work, to reduce the interfacial resistance, $LiTaO_3$ coating material was simply mixed with the solid electrolyte to measure the effect of suppressing side reactions. To synthesize the solid electrolyte $Li_{5.3}PS_{4.3}Cl_{1.7}$ and the mixing material $LiTaO_3$, high-energy ball milling and wet milling methods were used, respectively. The structural characteristics of the prepared solid electrolytes were studied by powder X-ray diffraction. The $LiTaO_3$ mixed solid electrolyte based ASSB showed a high discharge capacity of 177.3mAh/g in the initial cycle, whereas the bare solid electrolyte ($Li_{5.3}PS_{4.3}Cl_{1.7}$) based ASSB showed a discharge capacity of 159.1mAh/g. To understand the side reactions, electrochemical impedance spectroscopy (EIS) analysis was performed after galvanostatic charging-discharging cycles. The EIS analysis confirmed that the side reaction between a solid electrolyte and a cathode has been effectively suppressed in $LiTaO_3$ mixed solid electrolyte based ASSBs.

Second, we prepared $Li_{5.3}PS_{4.3}Cl_{1.7}$ mixed with InF_3. We also confirm the structural properties using powder X-ray diffraction (XRD). Through the XRD pattern, it was observed that the argyrodite structure was maintained and only the intensity of the peak corresponding to InF_3 increased. The optimized solid electrolyte based ASSB showed a higher initial discharge

capacity of 172.8mAh/g and a coulombic efficiency of 78.54%, and the capacity retention rate was also measured to be better than bare solid electrolyte ($Li_{5.3}PS_{4.3}Cl_{1.7}$) based ASSB.

Contents

List of Tables

List of Figures

Chapter 1. Introduction

1-1. Lithium ion secondary batteries

Lithium secondary batteries are used in various fields such as electric vehicles as well as small electronic devices such as mobile phones, tablets, and laptops. In particular, as carbon neutral policies are implemented globally, the importance of batteries is growing. However, liquid electrolyte, one of the components of lithium secondary batteries, uses organic solvents, so there are risks of corrosion, temperature vulnerability, leakage, and explosion. In fact, explosion accidents due to battery thermal runaway are occurring in many electric vehicles and smartphones. To solve this problem, researchers are trying to develop materials that are safer than existing liquid electrolytes.

1-1-1. Composition of lithium ion batteries

A lithium secondary battery consists of a cathode, anode, separator, and electrolyte. In general, the conventional cathode materials involving intercalation and extraction of lithium ions with 1-D olivine ($LiFePO_4$), 2-D layered ($LiCoO_2$), and 3-D spinel ($LiMn_2O_4$) structures as shown in Figure 1.1. Typically, $LiCoO_2$ have been used due to its working voltage (3.0-4.5V vs. Li/Li^+) and good cycle life (>500 cycles). The properties of various cathode materials used in lithium-ion batteries are shown in Table 1.1. Representative anode materials include graphite, silicon, and lithium metal. Graphite has a low theoretical specific capacity of 372 mAh g^{-1}. Silicon theoretically has a specific capacity of 4200 mAg^{-1}, but undergoes significant volume expansion through repeated charging and discharging processes, causing cracks to form on the surface. Li metal has the advantage of having a theoretical specific capacity of 3860 mAh g^{-1} and the lowest electrochemical potential of -3.040 V compared to a standard hydrogen electrode. The separator prevents internal short circuit between the anode and cathode and allows only ions to pass through. The materials of the separator are mainly porous polyethylene and polypropylene. Organic liquid electrolyte materials such as ethylene carbonate-dimethyl carbonate (EC-DMC) with lithium salts are used due to their high ionic conductivity and stability over a wide range of voltage windows (0-4.5 V vs. Li/Li^+).

1-1-2. Principle of lithium ion batteries

The operating principle of a lithium secondary battery is shown in Figure 1.2. A secondary battery refers to a battery that can be charged and discharged and used repeatedly. For example, the cathode and anode are oxidized and reduced respectively during the charging step. The chemical reaction during charging and discharging can be expressed by the following equation:

Cathode: $LiCoO_2 \leftrightarrow Li_{1-x}CoO_2 + xLi + xe^-$ (1.1)

Anode: $C_6 + xLi + xe^- \leftrightarrow Li_xC_6$ (1.2)

Overall: $LiCoO_2 + C_6 \leftrightarrow Li_{1-x}CoO_2 + Li_xC_6$ (1.3)

Lithium ions move from the cathode to the anode through the electrolyte when charging, and the direction is reversed when discharging. To balance the charge, the direction of electron movement is the same as that of lithium ions, and electrons move through the external conductor rather than through the electrolyte. Electrons travel through an external circuit connected to the current collector. Chemical energy generated by a chemical reaction can be converted into electrical energy and stored according to the Nernst equation.

$$\Delta G = -nFE \quad (1.4)$$

G is the Gibbs energy, n is the number of electrons required for the reaction, F is the Faraday constant, and E is the electric potential. From the above equation, we can see that the greater the chemical potential difference between the cathode and anode, the greater the potential and energy. The electric potential proportional to the chemical energy is called to the open circuit voltage (OCV) and is determined within the band gap of the electrolyte, which is determined by the difference in energy between the highest occupied molecular orbital (HOMO) and the lowest unoccupied molecular orbital (LUMO) of the electrolyte as shown in Figure 1.3 [1-3].

1-1-3. Properties and limitation of organic liquid electrolyte

Commercially used organic liquid electrolytes usually consist of 1M $LiFP_6$ mixed with two or more carbonate-based materials and ethyl carbonate (EC)/dimethyl carbonate (DMC) in a

1:1 ratio. General organic solvent electrolytes have superior dielectric constant and electrochemical stability compared to aqueous electrolytes, so they have been applied to many lithium batteries. In order to apply electrolytes to large-scale energy devices, several conditions must be met [4].

1) Maintain SEI during charging and discharging
2) A Li+ ion conductivity $\sigma_{Li} > 10^{-4} S/cm$
3) An electronic conductivity $\sigma_e < 10^{-10} S/cm$
4) A transference number $\sigma_{Li}/\sigma_{total} \approx 1$, where σ_{total} includes conductivities by other ions in the electrolyte
5) Chemical stability over wide temperature ranges

Organic liquid electrolytes have the disadvantages of low transition number, chemical stability, and electrochemical stability. In general, lithium salt electrolytes have poor high-speed performance due to low lithium ion mobility, and have limitations in output due to problems such as solvation and dissociation [1]. However, the most important issues to address are safety and liquid leakage issues related to thermal stability. Organic electrolytes have another problem called temperature vulnerability, so they can decompose at high temperatures. As lithium batteries expand, not only does the internal pressure increase, but there is also a risk of explosion when the cathode and anode meet, causing an internal short circuit. To solve this problem, various types of electrolytes have been developed, such as gel electrolytes and solid electrolytes that do not leak and have excellent thermal and electrochemical stability.

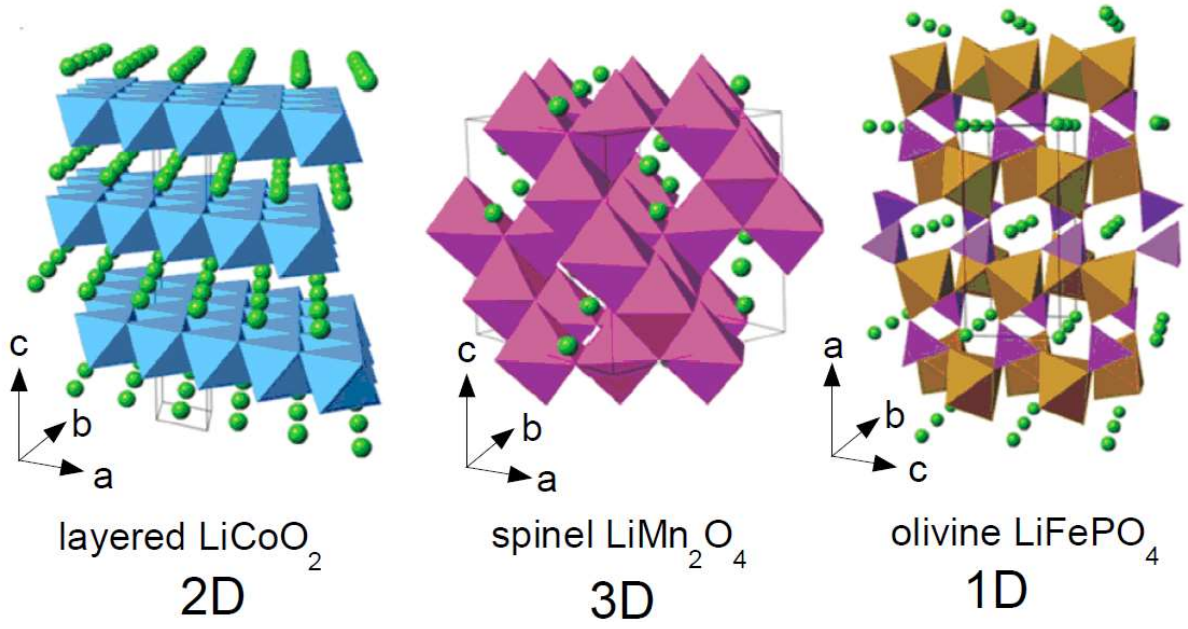

Figure 1.1. Crystal structures of the three lithium-insertion compounds in which the Li^+ ions are mobile through the 2-D (layered), 3-D (spinel) and 1-D (olivine) frameworks.

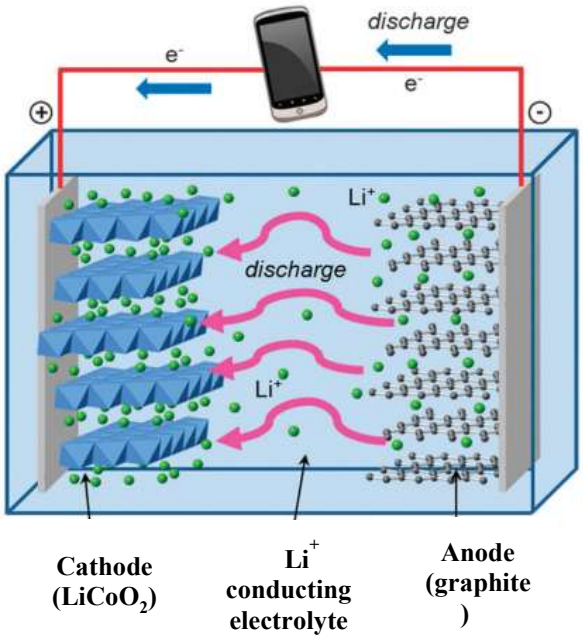

Figure 1.2. Illustration of operating principle of lithium secondary battery system.

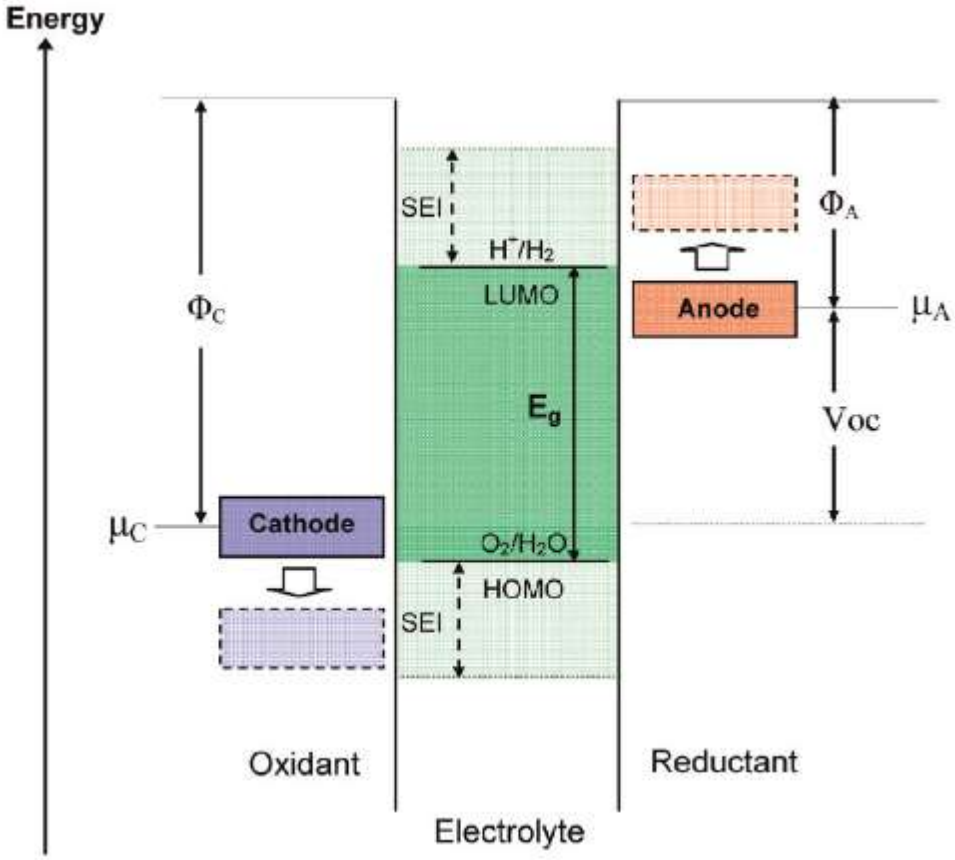

Figure 1.3. Schematic open-circuit energy diagram of a lithium cell.

1-2. All-solid-state lithium ion batteries

Lithium-ion batteries are widely used not only in small electronic devices such as smartphones and tablets, but also in large devices such as electric vehicles and ESS [5]. Conventional organic liquid electrolytes commonly used in lithium-ion batteries have various problems such as leakage, temperature vulnerability, and corrosion, which poses safety problems [6]. Therefore, attempts are being made to solve existing problems by replacing liquid electrolytes with solid electrolytes. Applying a solid electrolyte to a battery not only ensures stability but also ensures high performance and high energy density of the battery [7]. Additionally, solid electrolytes have received much attention due to their potential for superior ionic conductivity and high lithium transfer numbers (~1) compared to aprotic electrolytes (0.2–0.5) [8, 9]. Among these advantages, solid electrolytes for large electrical devices have been intensively studied due to their attractive safety advantages such as electrochemical and thermal stability [1, 2]. Solid electrolytes are largely divided into inorganic materials and polymers. Polyelectrolytes have good flexibility and can be used in flexible batteries or devices. However, poor mechanical properties and low ionic conductivity preclude these electrolytes from practical applications. Therefore, research on inorganic solid electrolytes is actively underway.

1-2-1. Inorganic/ceramic solid electrolyte

Inorganic solid electrolytes have advantages such as strong mechanical strength and excellent ionic conductivity compared to polymer electrolytes. Representative types include perovskite, anti-perovskite, LISICON type, NASICON type, argyrodite, and garnet [10].

1-2-2. Properties of inorganic/ceramic solid electrolyte

Before commercialization, the inorganic solid electrolytes meet the following requirements:

1) Strong mechanical strength

2) Chemical stability from thermal decomposition [11] and flammable [12]

3) High ionic conductivity due to high lithium transference number (~1) compared to aprotic electrolytes (0.2-0.5) [8]

4) Stable electrochemical stability window [13]

5) Excellent compatibility with lithium metal batteries due to Li dendrite suppression properties suppression properties [14]

6) Eco-friendly comparing with organic carbonate base electrolytes

Inorganic electrolytes almost satisfy mechanical strength, chemical stability, non-flammability, Li dendrite suppression, and eco-friendliness. In particular, the improved stability and safety of inorganic solid electrolytes can easily and simply provide new designs for all-solid-state battery cells. Moreover, the solid electrolytes have high lithium transference number ($\sigma_{Li}/\sigma_{total}$), which reduces the effect of concentration polarization by precipitation of dissolved salts in the anode and depletion at the cathode [8], compared to liquid electrolytes containing aprotic and lithium salt ions , because they operate only by Li+ migration. As a result, the lifespan and safety of lithium-ion batteries are improved [10]. The electrochemical stability range of many inorganic electrolytes is known to be stable and wide. Most oxide electrolytes showed stable cathode stability across the cathode voltage range (5–9 V vs. Li+/Li) and, unlike liquid organic electrolytes, did not induce autolysis during charging and discharging. As a result, the solid electrolyte can suppress repetition of SEI formation and Li+ consumption, ultimately extending the lifespan of the lithium secondary battery.

1-2-3. Li^+ diffusion mechanism of inorganic/ceramic solid electrolyte

Inorganic solid electrolytes are composed of mobile ions such as Li^+, as well as non-metallic ligands and central metals that constitute the polyhedron (4, 6, 8, and 12-fold coordination) forming the framework of the crystal structures. Polyhedrons are ordered regularly by sharing such as corner or edge sharing, and form the Li^+ tunnels called bottlenecks with interstitials between large anions and vacancy from incomplete crystallinity of the solid material due to

thermodynamic stabilization [8, 15]. In the solid electrolytes, the lithium ions are diffused by migration through bottlenecks of the crystal structure, whereas liquid electrolytes involve the movement of solvated lithium ions in a solvent medium [8]. The migration divided into Schottky migration and Frenkel migration. In the case of Schottky migration, lithium ions move randomly to vacancies. In contrast, Frenkel migration occurs when lithium ions diffuse directly into the interstitial between the anions and the exchange interstitial sites [10]. When comparing the activation energy of migration, the Frenkel migration mechanism requires lower activation energy than Schottky migration. As a result, the Li^+ conductivity depends on the size and number of bottlenecks [16]. Interstitial and vacancy sites depend on the lattice parameters of the unit cell in structures with Li^+ concentrations. Also, the parameters are changed by the valence and size of the mobile ion [8]. For example, the repulsion between the same charge ions increases with increasing ion size and creates a larger bottleneck size and interstitial. For the ionic valence effect, the ionic conductivity decreases with increasing valence because the electrostatic interaction between the mobile ion and the counter-charged ion increases and ionic diffusion decreases.

1-3. Inorganic electrolyte

1-3-1. Oxide solid electrolyte

Oxide-based solid electrolytes for all-solid-state batteries have low ionic conductivity, however, good chemical and mechanical stability, and in particular, many studies have been conducted due to their stability in the atmosphere. Most oxide-based solid electrolytes produced have focused on using NASICON, perovskite, garnet, and LISICON structures.

NASICON-like structures are generally known as a rhombohedral unit cell and $R\bar{3}c$ with a few monoclinic and orthorhombic phases [17]. Representatively, $L_{1+6x}M_{4+2-x}M'_{3+x}(PO_4)_3$ phosphates (L = Li or Na and M =Ti, Ge, Sn, Hf, or Zr and M′ = Cr, Al, Ga, Sc, Y, In, or La) are composed with MO_6 octahedra connected by corner sharing with PO_4 tetrahedral to form 3D interconnected channels and two types of interstitial positions where mobile cations are distributed [18]. The M1 sites which are 6-fold coordination located between two MO_6 octahedral while M2 sites that are 8-fold coordinated and located between two columns of MO_6 octahedral [19]. The lithium ions diffuse from on site to another through bottlenecks. However,

the NASICON electrolytes containing Ti are unstable with Li metal at low potentials [20].

Perovskite materials having chemical formula ABO_3 is well known as the representative cubic phase with space group $Pm\bar{3}m$. Among the structural materials, lithium-lanthanum-titanates, $Li_{3x}La_{2/(3-x)}TiO_3$ (LLTO), is representative material due to its high ionic conductivity at room temperature (10^{-3} S/cm) [10]. The A site cations, which were Li^+ and La^{3+} in the cubic α-phase, were randomly distributed, while the A sites of the ordered β-LLTO had a doubled perovskite structure, with an alternating arrangement of La^+ rich and Li vacancy rich layers along the c axis [21]. Not only high ionic conductivity, the materials have many advantages such as stability in air and moisture, wide stability temperature window (to 1600K), good electrochemical stability (>8V). However, the materials have difficult to applied to commercial solid battery system because of its unsuitable for use with lithium and graphite negative electrodes [3, 10], high temperature sintering for synthesis and lower ionic conductivity than single crystal due to blocking grain boundaries [22].

The garnets exhibit a general chemical formula of $A_3B_2(XO_4)_3$ (A = Ca, Mg, Y, La or rare earth; B = Al, Fe, Ga, Ge, Mn, Ni or X = Si, Ge, Al) where A, B and C are eight, six and four oxygen coordinated cation sites, which crystalize in a face centered cubic structure with the space group $Ia\bar{3}d$ [23]. Because the garnet electrolytes high Li^+ concentration 5~7 Li atoms per formula unit and can accommodate excess Li^+ at octahedral sites than that of number of lithium at the tetrahedral sites [23], the ionic conductivity of the electrolytes can be controlled by increasing Li concentration. For example, $Li_5La_3M_2O_{12}$ have low ionic conductivity of 10^{-6} S/cm at room temperature. However, the low conductivity can be improved by substituting La and M sites with cations in an oxidation state higher or lower than La^{3+} and M^{5+} controlling the content of substitution elements such as $Li_{6.6}La_3Zr_{1.6}Sb_{0.4}O_{12}$ (7.7 x 10^{-4} S/cm) and $Li_{6.2}La_3Zr_{1.2}Sb_{0.8}O_{12}$ (4.5 x 10^{-4} S/cm) [24, 25]. Also, ionic conductivity of the garnet electrolytes can be improved by controlling shape control. For example, the particle shape of $Li_7La_3Zr_2O_{12}$ changes by contents of substitution element (Ga), and can be more dense pellets with same pressure [26]. As the results, the interface resistance by grain boundary was reduced. Although garnet electrolytes have high lithium concentration and ionic conductivity, the materials couldn`t be commercialized because of their unstable reactivity with cathode materials at the positive voltage window [27].

The crystal structure of LISICON-like compounds is related to the γ-Li_3PO_4 structure with

orthorhombic unit cell and *pnma* space group, where all cations are tetrahedral coordinated [10, 28]. The oxide LISICON-like materials such as $Li_{14}ZnGe_4O_{16}$ showed low ionic conductivity (~10^{-7} S/cm) at room temperature by trapping of the mobile Li^+ ions by the immobile sublattice at lower temperatures via the formation of defect complexes [20]. And the LISICON structures such as $Li_{3x}La_{2/3-x}TiO_3$ and $Li_{3/8}Sr_{7/16}Zr_{1/4}Ta_{3/4}O_3$, have low contact with Li metal due to the reduction of Ti and Ta ions.

Recently, thio-LISICON, which has been changed from O^{2-} to S^{2-} have been studied for high lithium ion conductivity at room temperature [10]. Many thio materials such as $Li_{10}MP_2S_{12}$ (M= Si, Ge, and Sn), $Li_{11}Si_2PS_{12}$ showed high ionic conductivity [29-31]. Especially, $Li_{10}GeP_2S_{12}$ showed highest lithium ion conductivity (~10^{-2} S/cm) at 27℃ [29] among current ceramic electrolytes [10]. As the radius of S^{2-} is higher than O^{2-}, this substitution can significantly enlarge the size of Li^+ transport bottlenecks. Also, S^{2-} has better polarization capability than O^{2-}. Consequently, the interaction between skeleton and Li^+ ion is weaker and make the mobility of Li^+ [32]. The thio-LISICON materials also have favorable advantage, which is reduction of grain boundary resistance by simple cold-press of electrolytes powders because of its good ductility compare with hard oxide materials [20].

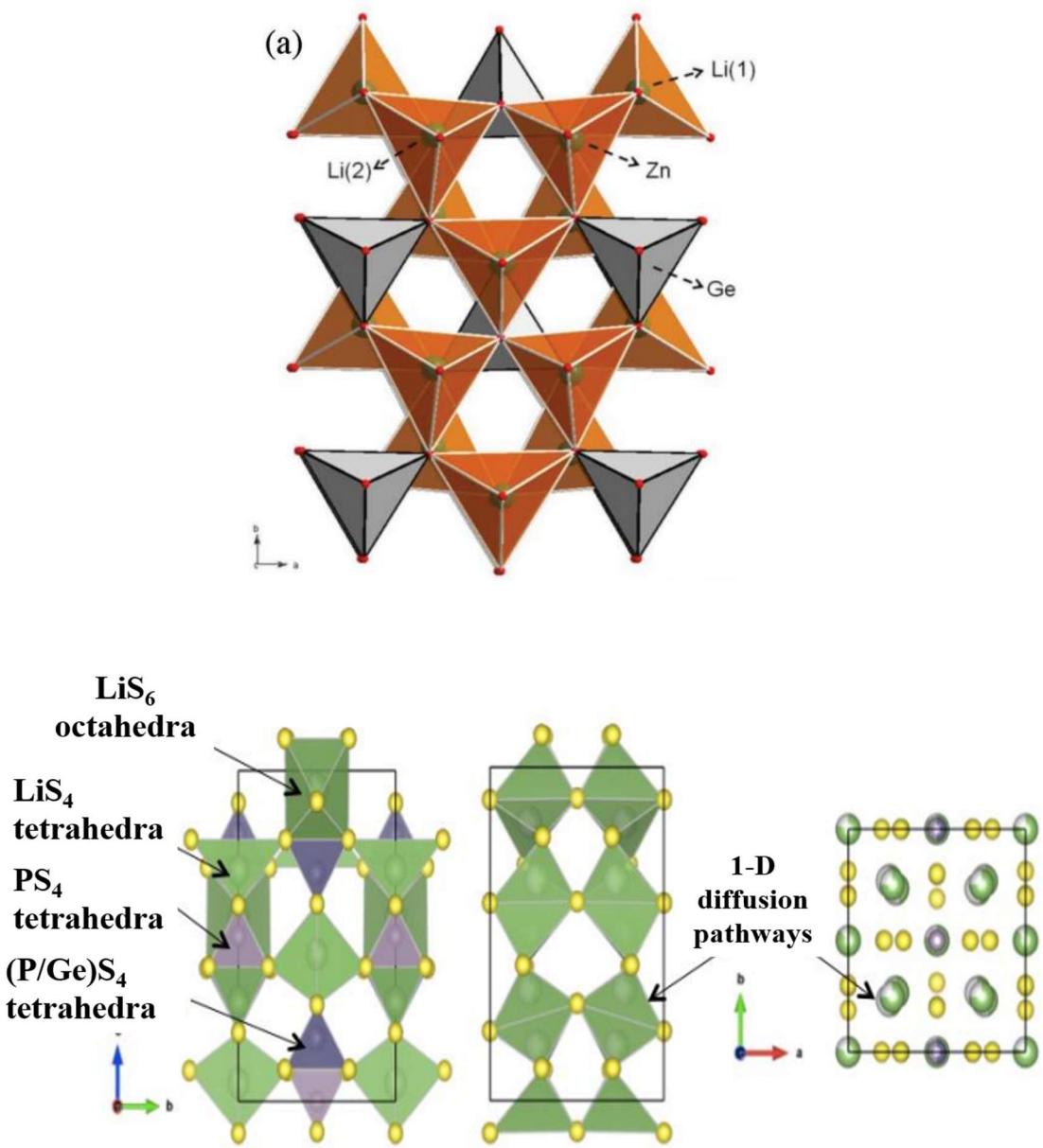

Figure 1.4. Schematic structure of LISICON-like.

1-3-2. Sulfide solid electrolyte

Sulfide-based solid electrolytes have small grain boundaries and good ductility, making them easy to process. However, because sulfide-based solid electrolytes react with moisture in the atmosphere and generate hydrogen sulfide gas, which is toxic to the human body, all processes must be performed in an environment where moisture is blocked. Nevertheless, sulfide-based solid electrolytes have higher ionic conductivity than oxide-based electrolytes because the polarization of sulfur ions is greater than that of oxygen ions, their electronegativity is low, and their binding force with lithium ions is low [33, 34]. The ionic radius of S^{2-} is larger than that of O^{2-}, so the ion transport channel is larger and the ion mobility is also greater [35]. Representative sulfide-based solid electrolytes currently being studied include thio-LISICON, Li_2S-P_2S_5 (LPS), and Li-argyrodite.

1-3-2-1. Thio-LISICON

Thio-LISICON materials such as $Li_{3.25}Ge_{0.25}P_{0.75}S_4$ and $Li_{10}GeP_2S_{12}$ have a wide electrochemical stability range from 0 V to 4 V compared to Li/Li^+ [36]. However, in the case of sulfide-based solid electrolytes, many results have been described showing that the electrochemical window is narrow and that they react with the cathode and anode [20, 31, 37, 38]. Because S^{2-} is larger and less electronegative than O^{2-}, the chemical interactions in the crystal structure of thio materials are weak. As a result, materials composed of S^{2-}anions have similar stability of less than 25 meV per atom and exhibit unstable characteristics compared to oxide materials. In LGPS systems, $Li_{10}GeP_2S_{12}$ electrolyte has received much attention due to its extremely high ionic conductivity of more than 10^{-2} S/cm. However, the amount of Ge existing in nature is limited, so research on replacing Ge with other elements is ongoing. In fact, most thio materials decompose by reacting with anode and cathode materials containing Li metal [38, 39]. Additionally, it is a material that is difficult to synthesize in the general atmosphere because it is very sensitive to air and moisture.

1-3-2-2. Li_2S-P_2S_5

Li_2S-P_2S_5 based glass-ceramics are of special interest due to their high ionic conductivity up to 1.7 x 10^{-2} S/cm at room temperature and their wide electrochemical window [40-44]. The Li_2S-P_2S_5 electrolyte is a metastable glass-ceramics with a (100-x)Li_2S-xP_2S_5 composition.

This metastable phase is formed through partial crystallization by heat treatment after formation of the glass electrolyte. According to each composition ratio, these metastable phases such as $Li_7P_3S_{11}$, β-Li_3PS_4, and thio-LISICON analog showed higher lithium ion conductivity than $Li_4P_2S_6$ which is the stable crystalline phase. Among them, $Li_7P_3S_{11}$ (LPS) glass-ceramic can be easily synthesized by methods such as ball milling and solution techniques that allow other components to be mixed with the LPS [45, 46]. The $Li_7P_3S_{11}$ electrolyte which has a composition ratio of Li_2S and P_2S_5 of 7:3 reduced the interfacial resistance through hot press and exhibited lithium ion conductivity of 10^{-2} S/cm. Moreover, the powder obtained after heat treatment can be easily applied to the fabrication of electrolytes for bulk type ASSLBs [47]. However, since the LPS electrolyte is very unstable, it reacts with the lithium anode and decomposes, and the interfacial resistance with lithium metal is large. Due to the reaction characteristics between LPS and Li metal, low coulombic efficiency and capacity degradation in all-solid-state batteries are caused, which limits the application of all-solid-state batteries [45].

1-3-2-3. Argyrodite

Argyrodite is a type of chalcogenide structure related to Ag_8GeS_6 minerals containing various fast Ag^+ or Cu^+ ion conductors, such as A_7PS_5X (A = Ag+, Cu+). Recently, Deiseroth et al. synthesized the analogue cubic Li^+ argyrodite with the formula Li_6PS_5X (X=Cl, Br, I) and Li_7PS_6. Li-argyrodite electrolyte is a lithium conductor with a structure similar to Ag_8GeS_6, which has a mineral argyrodite structure. Lithium argyrodite electrolyte has a structure in which silver ions in the mineral argyrodite structure are replaced with lithium ions because the atomic radii of silver and lithium ions are similar and have the same coordination number. ion diffusion proceeds through randomly generated specific atomic positions [48, 49].

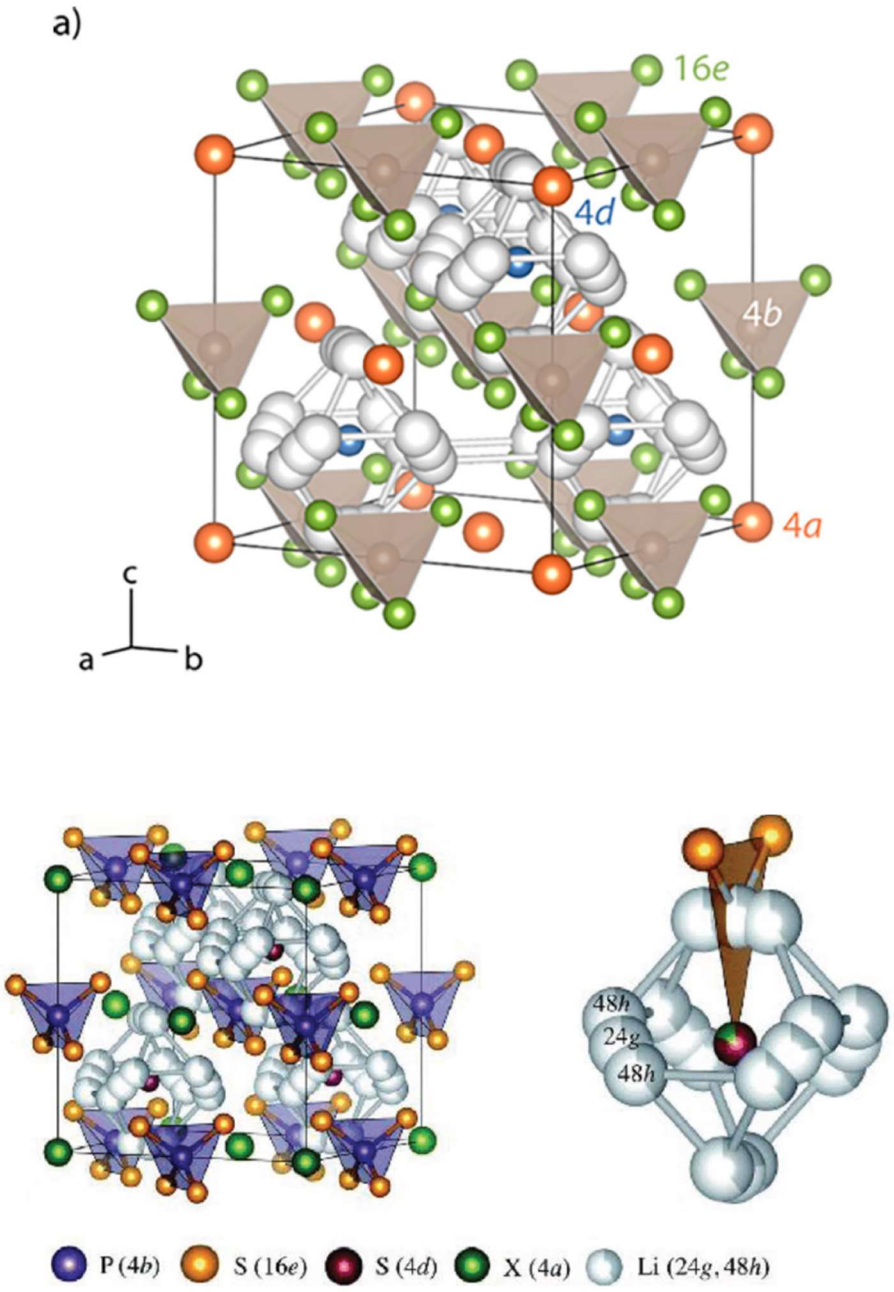

Figure 1.5. Crystal structure of argyrodite-type Li_6PS_5X.

1-4. Reference

[1] Minh, Nguyen Q. "Ceramic fuel cells." *Journal of the American Ceramic Society* 76, no. 3 (1993): 563-588.

[2] Tarascon, J-M., and Michel Armand. "Issues and challenges facing rechargeable lithium batteries." In *Materials for sustainable energy: a collection of peer-reviewed research and review articles from Nature Publishing Group*, pp. 171-179. 2011.

[3] Stephan, A. Manuel, and K. S. Nahm. "Review on composite polymer electrolytes for lithium batteries." *Polymer* 47, no. 16 (2006): 5952-5964.

[4] Xu, Kang. "Nonaqueous liquid electrolytes for lithium-based rechargeable batteries." *Chemical reviews* 104, no. 10 (2004): 4303-4418.

[5] Seino, Yoshikatsu, Tsuyoshi Ota, Kazunori Takada, Akitoshi Hayashi, and Masahiro Tatsumisago "A sulphide lithium super ion conductor is superior to liquid ion conductors for use in rechargeable batteries" Energy & Environmental Science 7, no. 2 (2014): 627-631.

[6] Zhang, Jicheng, Rui Gao, Limei Sun, Heng Zhang, Zhongbo Hu, and Xiangfeng Liu "Unraveling the multiple effects of Li_2ZrO_3 coating on the structural and electrochemical performances of $LiCoO_2$ as high-voltage cathode materials" *Electrochimica Acta* 209 (2016): 102-110.

[7] Wenzel, Sebastian, Dominik A. Weber, Thomas Leichtweiss, Martin R. Busche, Joachim Sann, and Jürgen Janek "Interphase formation and degradation of charge transfer kinetics between a lithium metal anode and highly crystalline $Li_7P_3S_{11}$ solid electrolyte." *Solid State Ionics* 286 (2016): 24-33.

[8] Xu, Kang "Nonaqueous liquid electrolytes for lithium-based rechargeable batteries" *Chemical Reviews* 104, no. 10 (2004): 4303-4418.

[9] Kamaya, Noriaki, Kenji Homma, Yuichiro Yamakawa, Masaaki Hirayama, Ryoji Kanno, Masao Yonemura, Takashi Kamiyama, Yuki Kato, Shigenori Hama, Koji Kawamoto and Akio Mitsui "A lithium superionic conductor" *Nature Materials* 10, no. 9 (2011): 682.

[10] Bachman, John Christopher, Sokseiha Muy, Alexis Grimaud, Hao-Hsun Chang, Nir Pour,

Simon F. Lux, Odysseas Paschos et al. "Inorganic solid-state electrolytes for lithium batteries: mechanisms and properties governing ion conduction." *Chemical reviews* 116, no. 1 (2016): 140-162.

[11] Goodenough, John B., and Youngsik Kim. "Challenges for rechargeable Li batteries." *Chemistry of materials* 22, no. 3 (2010): 587-603.

[12] Dyer, Chris K., Patrick T. Moseley, Zempachi Ogumi, David AJ Rand, and Bruno Scrosati, eds. *Encyclopedia of Electrochemical Power Sources*. Elsevier Science & Technology., 2009.

[13] Jung, Yun-Chae, Seul-Ki Kim, Moon-Sung Kim, Jeong-Hye Lee, Man-Seok Han, Duck-Hyun Kim, Woo-Cheol Shin, Makoto Ue, and Dong-Won Kim. "Ceramic separators based on Li^+-conducting inorganic electrolyte for high-performance lithium-ion batteries with enhanced safety." *Journal of Power Sources* 293 (2015): 675-683.

[14] Garche, Jurgen, Chris K. Dyer, Patrick T. Moseley, Zempachi Ogumi, David AJ Rand, and Bruno Scrosati, eds. *Encyclopedia of electrochemical power sources*. Newnes, 2013.

[15] A. Martínez-Juárez, C. Pecharromán, J. E. Iglesias, and J. M. Rojo, "Relationship between activation energy and bottleneck size for Li^+ ion conduction in NASICON materials of composition $LiMM'(PO_4)_3$; M, M′ = Ge, Ti, Sn, Hf," *J. Phys. Chem. B*, vol. 102, no. 2, pp. 372–375, 1998.

[16] J. B. Goodenough, "Oxide-ion electrolytes," *Annu. Rev. Mater. Res.*, vol. 33, pp. 91–128, 2003.

[17] Aono, Hiromichi, Eisuke Sugimoto, Yoshihiko Sadaoka, Nobuhito Imanaka, and Gin-ya Adachi. "The electrical properties of ceramic electrolytes for $LiMxTi_{2-x}(PO_4)_{3+y}Li_2O$, M= Ge, Sn, Hf, and Zr systems." *Journal of The Electrochemical Society* 140, no. 7 (1993): 1827-1833.

[18] Ortiz, Gregorio F., María C. López, Pedro Lavela, Candela Vidal-Abarca, and José L. Tirado. "Improved lithium-ion transport in NASICON-type lithium titanium phosphate by calcium and iron doping." *Solid State Ionics* 262 (2014): 573-577.

[19] Norhaniza, R., R. H. Y. Subban, and N. S. Mohamed. "Cr and V substituted LiSn2P3O12

solid electrolyte materials." *Journal of power sources* 244 (2013): 300-305.

[20] Cao, Can, Zhuo-Bin Li, Xiao-Liang Wang, Xin-Bing Zhao, and Wei-Qiang Han. "Recent advances in inorganic solid electrolytes for lithium batteries." *Frontiers in Energy Research* 2 (2014): 25.

[21] Hartmann, Pascal, Thomas Leichtweiss, Martin R. Busche, Meike Schneider, Marisa Reich, Joachim Sann, Philipp Adelhelm, and Jürgen Janek. "Degradation of NASICON-type materials in contact with lithium metal: formation of mixed conducting interphases (MCI) on solid electrolytes." *The Journal of Physical Chemistry C* 117, no. 41 (2013): 21064-21074.

[22] Wenzel, Sebastian, Thomas Leichtweiss, Dominik Krüger, Joachim Sann, and Jürgen Janek "Interphase formation on lithium solid electrolytes-An in situ approach to study interfacial reactions by photoelectron spectroscopy." *Solid State Ionics* 278 (2015): 98-105.

[23] Thangadurai, Venkataraman, Sumaletha Narayanan, and Dana Pinzaru. "Garnet-type solid-state fast Li ion conductors for Li batteries: critical review." *Chemical Society Reviews* 43, no. 13 (2014): 4714-4727.

[24] Cussen, Edmund J. "Structure and ionic conductivity in lithium garnets." *Journal of Materials Chemistry* 20, no. 25 (2010): 5167-5173.

[25] Ramakumar, S., L. Satyanarayana, Sunkara V. Manorama, and Ramaswamy Murugan. "Structure and Li+ dynamics of Sb-doped $Li_7La_3Zr_2O_{12}$ fast lithium ion conductors." *Physical Chemistry Chemical Physics* 15, no. 27 (2013): 11327-11338.

[26] El Shinawi, Hany, and Jürgen Janek. "Stabilization of cubic lithium-stuffed garnets of the type "$Li_7La_3Zr_2O_{12}$" by addition of gallium." *Journal of power sources* 225 (2013): 13-19.

[27] Kim, Ki Hyun, Yasutoshi Iriyama, Kazuo Yamamoto, Shota Kumazaki, Toru Asaka, Kinuka Tanabe, Craig AJ Fisher, Tsukasa Hirayama, Ramaswamy Murugan, and Zempachi Ogumi. "Characterization of the interface between $LiCoO_2$ and $Li_7La_3Zr_2O_{12}$ in an all-solid-state rechargeable lithium battery." *Journal of Power Sources* 196, no. 2 (2011): 764-

767.

[28] West, A. R. "Crystal chemistry of some tetrahedral oxides." *Zeitschrift für Kristallographie-Crystalline Materials* 141, no. 1-6 (1975): 422-436.

[29] Bron, Philipp, Sebastian Johansson, Klaus Zick, Jörn Schmedt auf der Günne, Stefanie Dehnen, and Bernhard Roling. "$Li_{10}SnP_2S_{12}$: an affordable lithium superionic conductor." *Journal of the American Chemical Society* 135, no. 42 (2013): 15694-15697.

[30] Kamaya, Noriaki, Kenji Homma, Yuichiro Yamakawa, Masaaki Hirayama, Ryoji Kanno, Masao Yonemura, Takashi Kamiyama et al. "A lithium superionic conductor." *Nature materials* 10, no. 9 (2011): 682-686.

[31] Kuhn, Alexander, Oliver Gerbig, Changbao Zhu, Frank Falkenberg, Joachim Maier, and Bettina V. Lotsch. "A new ultrafast superionic Li-conductor: ion dynamics in $Li_{11}Si_2PS_{12}$ and comparison with other tetragonal LGPS-type electrolytes." *Physical Chemistry Chemical Physics* 16, no. 28 (2014): 14669-14674.

[32] Murayama, Masahiro, Ryoji Kanno, Michihiko Irie, Shinya Ito, Takayuki Hata, Noriyuki Sonoyama, and Yoji Kawamoto. "Synthesis of new lithium ionic conductor thio-LISICON—lithium silicon sulfides system" *Journal of Solid State Chemistry* 168, no. 1 (2002): 140-148.

[33] Muramatsu, Hiromasa, Akitoshi Hayashi, Takamasa Ohtomo, Sigenori Hama, and Masahiro Tatsumisago "Structural change of Li_2S–P_2S_5 sulfide solid electrolytes in the atmosphere" *Solid State Ionics* 182, no. 1 (2011): 116-119.

[34] Ohtomo, Takamasa, Akitoshi Hayashi, Masahiro Tatsumisago, and Koji Kawamoto "Suppression of H_2S gas generation from the $75Li_2S{\cdot}25P_2S_5$ glass electrolyte by additives" *Journal of Materials Science* 48, no. 11 (2013): 4137-4142.

[35] Tatsumisago, Masahiro, and Akitoshi Hayashi "Sulfide Glass-Ceramic Electrolytes for All Solid-State Lithium and Sodium Batteries" *International Journal of Applied Glass Science* 5, no. 3 (2014): 226-235.

[36] Kanno, Ryoji, and Masahiro Murayama. "Lithium ionic conductor thio-LISICON: the $Li_2SGeS_2P_2S_5$ system." *Journal of the electrochemical society* 148, no. 7 (2001): A742-A746.

[37] Rao, R. Prasada, and S. Adams. "Studies of lithium argyrodite solid electrolytes for all-solid-state batteries." *physica status solidi (a)* 208, no. 8 (2011): 1804-1807.

[38] Mo, Yifei, Shyue Ping Ong, and Gerbrand Ceder. "First principles study of the $Li_{10}GeP_2S_{12}$ lithium super ionic conductor material." *Chemistry of Materials* 24, no. 1 (2012): 15-17.

[39] Chung, Habin, and Byoungwoo Kang. "Increase in grain boundary ionic conductivity of $Li_{1.5}Al_{0.5}Ge_{1.5}(PO_4)_3$ by adding excess lithium." *Solid State Ionics* 263 (2014): 125-130.

[40] Liu, D., W. Zhu, Z. Feng, A. Guerfi, A. Vijh, and K. Zaghib "Recent progress in sulfide-based solid electrolytes for Li-ion batteries" *Materials Science and Engineering: B* 213 (2016): 169-176.

[41] Che, Haiying, Suli Chen, Yingying Xie, Hong Wang, Khalil Amine, Xiao-Zhen Liao, and Zi-Feng Ma "Electrolyte design strategies and research progress for room-temperature sodium-ion batteries" *Energy & Environmental Science* 10, no.5 (2017): 1075-1101.

[42] Chen, Long, Yutao Li, Shuai-Peng Li, Li-Zhen Fan, Ce-Wen Nan, and John B. Goodenough "PEO/garnet composite electrolytes for solid-state lithium batteries: from "ceramic-in-polymer" to "polymer-in-ceramic"" *Nano Energy* 46 (2018): 176-184.

[43] Owejan, Jeanette E., Jon P. Owejan, Steven C. DeCaluwe, and Joseph A. Dura "Solid electrolyte interphase in Li-ion batteries: evolving structures measured in situ by neutron reflectometry" *Chemistry of Materials* 24, no. 11 (2012): 2133-2140.

[44] Tan, Guoqiang, Feng Wu, Chun Zhan, Jing Wang, Daobin Mu, Jun Lu, and Khalil Amine "Solid-state li-ion batteries using fast, stable, glassy nanocomposite electrolytes for good safety and long cycle-life" *Nano Letters* 16, no. 3 (2016): 1960-1968.

[45] Mo, Shanshan, Penghao Lu, Fei Ding, Zhibin Xu, Jiaquan Liu, Xingjiang Liu, and Qiang Xu "High-temperature performance of all-solid-state battery assembled with 95(0.7 Li_2S-0.3 P_2S_5)-5Li_3PO_4 glass electrolyte" *Solid State Ionics* 296 (2016): 37-41.

[46] Ohtomo, Takamasa, Akitoshi Hayashi, Masahiro Tatsumisago, Yasushi Tsuchida, Shigenori Hama, and Koji Kawamoto "All-solid-state lithium secondary batteries using the $75Li_2S{\cdot}25P_2S_5$ glass and the $70Li_2S{\cdot}30P_2S_5$ glass–ceramic as solid

electrolytes" *Journal of Power Sources* 233 (2013): 231-235.

[47] Lü, Xujie, John W. Howard, Aiping Chen, Jinlong Zhu, Shuai Li, Gang Wu, Paul Dowden, Hongwu Xu, Yusheng Zhao, and Quanxi Jia "Antiperovskite Li_3OCl Superionic Conductor Films for Solid-State Li-Ion Batteries" *Advanced Science* 3, no. 3 (2016): 1500359.

[48] R. B. Beeken, J. J. Garbe, J. M. Gillis, N. R. Petersen, B. W. Podoll, and M. R. Stoneman, "Electrical conductivities of the Ag_6PS_5X and the Cu_6PSe_5X (X=Br, I) argyrodites," *J. Phys. Chem. Solids*, vol. 66, no. 5, pp. 882–886, 2005.

[49] H.-J. Deiseroth *et al.*, "Li_6PS_5X: A Class of Crystalline Li-Rich Solids With an Unusually High Li^+ Mobility," *Angew. Chemie*, vol. 120, no. 4, pp. 767–770, 2008.

Chapter 2. $LiTaO_3$ mixing effects to suppress side reactions at the $LiNi_{0.8}Co_{0.1}Mn_{0.1}O_2$ cathode and $Li_{5.3}PS_{4.3}Cl_{1.7}$ solid electrolyte of all-solid-state lithium batteries

2-1. Introduction

In the modern world, lithium-ion batteries (LIB) have come to be widely used in everything from portable electronic devices to electric vehicles and energy storage systems. In particular, as carbon neutral policies continue to be implemented globally, demand for lithium secondary batteries has been rapidly increasing worldwide [1–3]. A liquid electrolyte is the type that is currently most often applied to lithium secondary batteries. As a liquid electrolyte is an organic solvent, it is flammable and highly reactive, which means there are various stability issues such as corrosion and temperature vulnerability must be resolved [4–7]. In this respect, solid electrolytes are advantageous in terms of battery performance such as safety, high energy density, high output, and long life, and they are also advantageous in terms of the fact that they involve a simplified manufacturing process, larger/compact batteries, and lower cost, which has led to solid electrolytes being researched and developed as next-generation secondary batteries [8–12]. Among the various types of solid electrolytes, the one that has attracted the most attention is the sulfide-based solid electrolyte.

Sulfide-based solid electrolytes have emerged as the most suitable option to replace liquid electrolytes because they show high ionic conductivity and good mechanical deformability [13, 14]. A representative sulfide-based solid electrolyte that exhibits particular high ionic conductivity is Li_6PS_5X (X=Cl, Br, I) [15, 16]. Kraft *et al.* studied how ionic conductivity changes when halogen anions are changed in a sulfide-based solid electrolyte [17]. They found that increasing the halide content from Li_6PS_5Cl to $Li_{5.5}PS_{4.5}Cl_{1.5}$ generated more Li^+ vacancies and increased Cl^-/S^{2-} site disorder, which can in turn increase ionic conductivity [18, 19]. However, most thiophosphate solid electrolytes exhibit low thermodynamic stability and a narrow electrochemical stability window. This becomes a problem at an interface with high-voltage cathode active materials such as $LiNi_{1-x-y}Co_xMn_yO_2$ (NCM) during battery assembly [20–23].

Coating an electrochemically stable material on the surface of cathode has been used as a method to suppress the side reactions occurring at interface between the solid electrolyte and the cathode [24–36]. Surface coating can significantly increase the capacity of an ASSB cathode [37]. Representative coating materials for this purpose include $LiNbO_3$ and $LiTaO_3$ [29–32]. Suitable coating materials for ASSB must have certain properties such as high ionic conductivity, low electronic conductivity, and low reactivity with sulfide electrolytes. When using the same coating amount and method, the effect of $LiTaO_3$ coating was similar to or superior to that of $LiNbO_3$ coating [37]. However, for effective suppression, the thickness of the coating film must be thin and uniform. An expensive ethoxide series must typically be used as a starting material to achieve uniform thinness [34–36]. Therefore, there have been a number of attempts to improve performance through the use of simple mixing [38, 39].

In the current study, $LiTaO_3$ coating material was simply mixed with $Li_{5.3}PS_{4.3}Cl_{1.7}$ with the aim of suppressing side reactions. To synthesize the solid electrolyte $Li_{5.3}PS_{4.3}Cl_{1.7}$ and the mixing material $LiTaO_3$, high-energy ball milling and wet milling methods were used, respectively. The ionic conductivity of the optimized composition was 5.32mS/cm at room temperature, and it showed a high critical current density of 0.65mA/cm^2 in DC cycling experiments with lithium metal. Further, when a solid electrolyte containing $LiTaO_3$ was used to create the cathode composite to construct the cell, it achieved a higher discharge capacity of 177.3mAh/g compared to when the cathode composite without $LiTaO_3$ was used.

2-2. Experimental

2-2-1. Synthesis of $LiTaO_3$ nanoparticles

First, $LiTaO_3$ nanoparticles were manufactured by wet milling method. Li_2CO_3 (99.0%, Sigma) and Ta_2O_5 (99%, Sigma) were used as starting materials, mixed at a 1:1 molar ratio, and hand-grinded for 15 minutes using a mortar [40]. The mixed precursor was transferred to a zirconia ball milling container and ethanol was added as mixing solvent. The ball milling process was carried out at a rotation speed of 300 rpm for 20 h (condition: 30 min run and 10 min rest). After ball milling process, the samples were dried in an oven at 60℃ for more than

3 hours. The dried product was then ground again for 15 minutes, sintered at 900℃ for 2 hours with the increasing heating rate of 2℃ min^{-1}, and lastly grinded again for 15 minutes to produce the final $LiTaO_3$ nanoparticles.

2-2-2. preparation of (100-x)$Li_{5.3}PS_{4.3}Cl_{1.7}$: x$LiTaO_3$ (x = 0, 2, 4, 6, and 8)

To synthesize $Li_{5.3}PS_{4.3}Cl_{1.7}$, Li_2S (99.98%, Sigma), P_2S_5 (99%, Sigma), and LiCl (99.9%, Sigma) were used as the starting precursors. To begin, the above precursors were weighed according to the stoichiometric ratio of the $Li_{5.3}PS_{4.3}Cl_{1.7}$ composition and uniformly grinded using a hand grinding process for 30 minutes in argon atmosphere. Next, the mixed powder was transferred to a zirconium jar that was then sealed, and a high energy ball milling process was performed at a speed of 500 rpm for 8 hours. After ball milling, the powder was pelletized at 20kN, sintered at 500℃ for 15 hours with an increasing heating rate of 2℃ min^{-1}, followed by hand grinding for 30 minutes to obtain the final solid electrolyte. $Li_{5.3}PS_{4.3}Cl_{1.7}$ and $LiTaO_3$ were then mixed through simple hand grinding for 15 minutes. $LiTaO_3$ was mixed in the solid electrolyte at ratios of 2, 4, 6, and 8 mol%. For comparison, $Li_{5.3}PS_{4.3}Cl_{1.7}$ without $LiTaO_3$ was also prepared. This synthesized pristine solid electrolyte, $Li_{5.3}PS_{4.3}Cl_{1.7}$, was named LPSCl, and the solid electrolytes prepared by mixing $LiTaO_3$ were named in ascending order of mixing ratio as 98LPSCl-2LTaO, 96LPSCl-4LTaO, 94LPSCl-6LTaO, and 92LPSCl-8LTaO, respectively.

2-2-3. Characterization and electrochemical performance measurements

Electrochemical Impedance Spectroscopy (EIS) was used to both determine the ionic conductivity of the synthesized solid electrolyte and analyze the resistance factor of ASSB. To determine the ionic conductivity of the synthesized solid electrolyte, solid electrolyte powder (250 mg) was placed in a mold with a diameter of 10 mm and then pressed at 20kN to pelletize it. At this point, indium foil was attached to both sides of the pellet to create an In/SE/In symmetrical cell. Using Biologic (Sp-300), alternating current (AC) was applied in the frequency range from 7 MHz to 1 Hz at an amplitude of 50 mV, and ionic conductivity was measured at room temperature (RT). Using the same method, EIS was measured from 30°C to 110°C at 10°C intervals to obtain the activation energy. To analyze the resistance factor of

ASSB, while again using Biologic (Sp-300), alternating current (AC) was applied in the frequency range from 7 MHz to 0.01 Hz at an amplitude of 50 mV.

Cyclic voltammetry (CV) was performed to evaluate the electrochemical stability window of the solid electrolyte. Solid electrolyte powder (200 mg) was placed in a mold with a diameter of 16 mm, and a Li/SE/SUS asymmetric 2032-type coin cell was constructed. The cell was lastly scanned at a rate of 1 mV/s from –0.5 V to 5.0 V at room temperature using a potentiostat/galvanostatic system (SP-300, BioLogic).

Next, DC analysis was conducted at room temperature to confirm the powder's compatibility with lithium metal. To this end, solid electrolyte powder (200 mg) was placed in a mold with a diameter of 16 mm and then pressed at 20kN to pelletize it. Li foil was attached to both sides of the pressed powder, and it was pressed again at 10kN to construct a Li/SE/Li coin cell. The critical current density of the cell was confirmed using a battery tester (Maccor, Thermotech Korea). The current density was increased by a step size of 0.05 mA/cm^2 from 0.05 mA/cm^2 to 0.80 mA/cm^2.

ASSB was made using the synthesized solid electrolyte, and its charge/discharge performance was tested. The cathode composite was prepared by mixing uncoated NCM811:solid electrolyte:VGNF in a respective ratio of 70:27:3 using a vortex mixer. In this assembly process, solid electrolyte powder (200 mg) was placed in a 16 mm diameter mold and pressed at 40kN to pelletize, after which 5.5 mg of cathode composite was evenly dispersed on the surface of the solid electrolyte pellet. Next, indium foil and a spacer were placed on top of the surface and cathode composite and pressed with 40kN, after which Li and a spacer were placed on the other side before pressing again with 7kN.At this point, the pellet was finally assembled in a 2032-type coin cell. The charge-discharge cycling tests were then analyzed at voltages ranging from 2.6-4.3 V (vs. Li/Li$^+$) with a current rate of 0.1C at 25℃ using the WonAtech WBCS 3000 battery test equipment.

2-3. Results and discussion

2-3-1. Structural characterization and morphology analysis of $LiTaO_3$ mixed with $Li_{5.3}PS_{4.3}Cl_{1.7}$ solid electrolyte

X-ray diffraction (XRD) was used to confirm the crystal structure of the solid electrolyte and the mixing of $LiTaO_3$ into the solid electrolyte. The XRD pattern of synthesized (100-x)$Li_{5.3}PS_{4.3}Cl_{1.7}$ – x$LiTaO_3$ (x=0, 2, 4, 6, and 8) is shown in Figure 2.1. Solid electrolytes of all compositions exhibit an argyrodite-type crystalline phase of cubic phase Li_7PS_6 (JCPDS-34-0688) with space group $\bar{F}43m$ [41–43]. The main diffraction peaks at 2θ = 15.4°, 17.8°, 25.4°, 29.8°, 31.2°, 39.7°, 44.9°, 47.7°, and 52.3° can be indexed to (111), (200), (220), (311), (222), (331), (422), (511), and (440) planes, respectively. The XRD pattern of synthesized $LiTaO_3$ is shown in Figure 2.2. Its XRD pattern is identical to that previously reported [44]. Through the XRD graph, there is no change in the argyrodite structure even when $LiTaO_3$ is introduced in solid electrolyte. When $LiTaO_3$ is mixed to x=2, the main peak of $LiTaO_3$ begins to appear separately from the peak corresponding to the argyrodite structure. Even if the mole fraction of $LiTaO_3$ increases, only the peak intensity of $LiTaO_3$ increases. This indicates that $LiTaO_3$ was not doped into the structure and only a simple mixing effect was achieved.

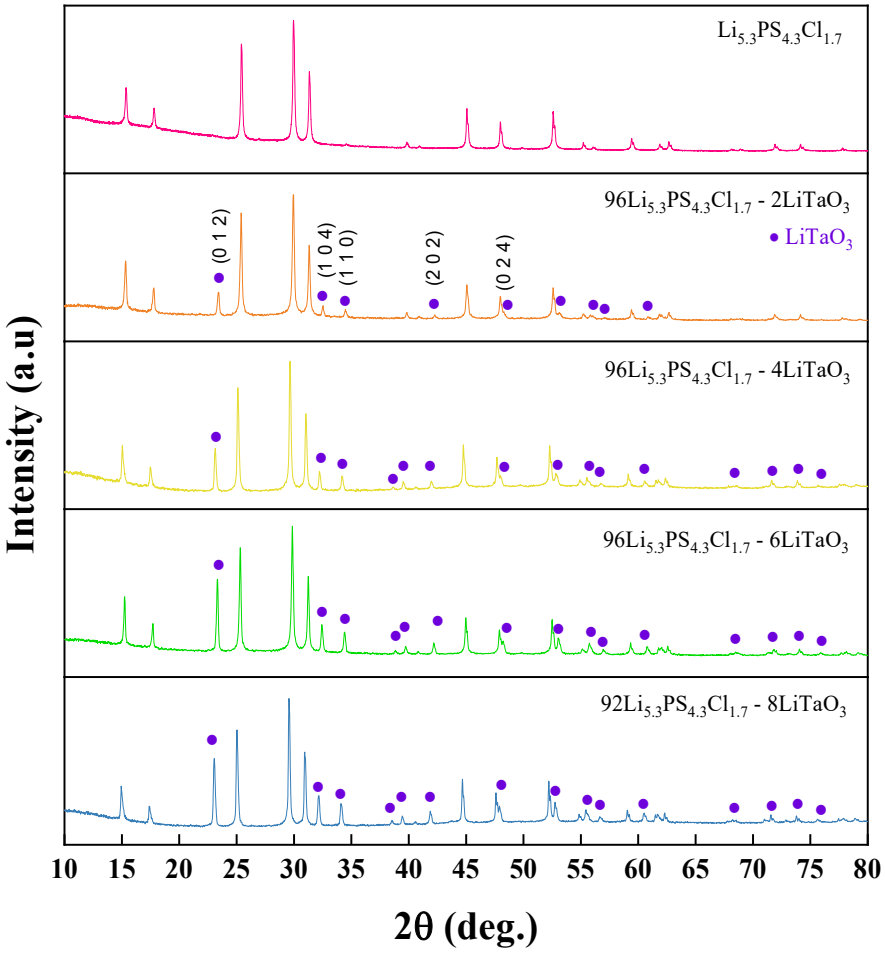

Figure 2.1. Powder X-ray diffraction patterns of (100-x)$Li_{5.3}PS_{4.3}Cl_{1.7}$ – x$LiTaO_3$ (x=0, 2, 4, 6, and 8) solid electrolytes.

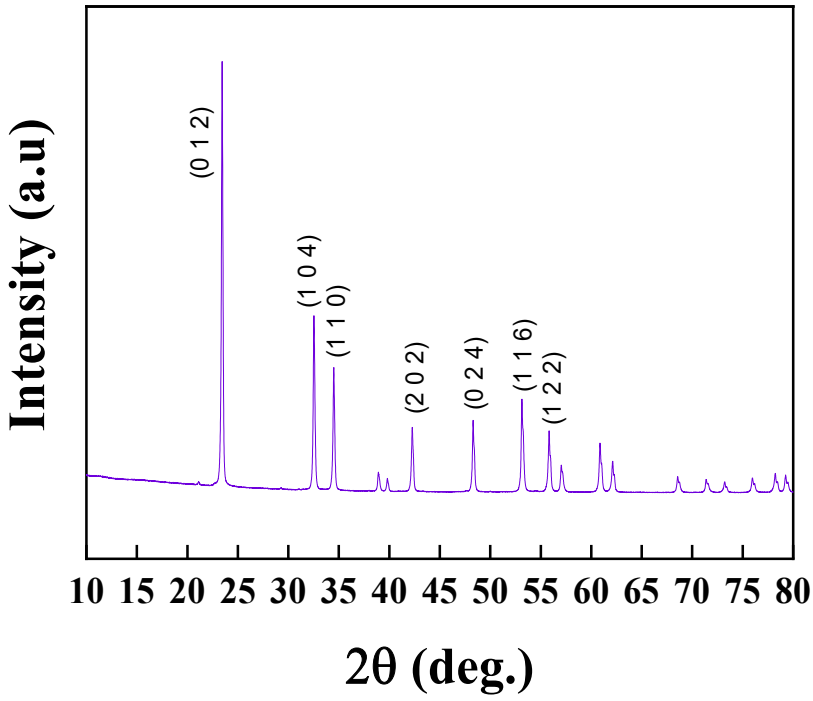

Figure 2.2. Powder X-ray diffraction patterns of synthesized $LiTaO_3$.

Figure 2.3 and Figure 2.4 show the SEM image and EDS mapping elemental distribution of the synthesized $LiTaO_3$ and solid electrolyte, respectively. Most $LiTaO_3$ particles are spherical and hundreds of nanometers in size. The distribution of Ta and O elements was mapped using EDS elemental analysis. The fact that the distribution forms of the two elements are consistent supports that $LiTaO_3$ was well synthesized. Meanwhile, the particle shape of $Li_{5.3}PS_{4.3}Cl_{1.7}$ is irregular and ranges in size from 1 to several micrometers. The consistent distribution patterns of P, S, and Cl elements support the fact that the solid electrolyte was well synthesized. The SEM image of the solid electrolyte mixed with $LiTaO_3$ in $Li_{5.3}PS_{4.3}Cl_{1.7}$ is shown in Figure 2.5(a-e). Unlike pristine $Li_{5.3}PS_{4.3}Cl_{1.7}$, it is observed that starting from x=2, small-sized $LiTaO_3$ particles are physically attached to the large-sized solid electrolyte surface. As the $LiTaO_3$ mole fraction increases, more $LiTaO_3$ tends to be observed on the surface of the solid electrolyte. Another important thing to note is that as the mixing ratio of $LiTaO_3$ increases, the degree of particle aggregation increases. This physical property affects the contact between particles and ion conduction. Figure 2.5(f) shows the EDS mapping image of the 94LPSCl-6LTaO composition. All elements are distributed uniformly without segregation or aggregation, suggesting that successful mixing of $LiTaO_3$ on $Li_{5.3}PS_{4.3}Cl_{1.7}$.

(a)

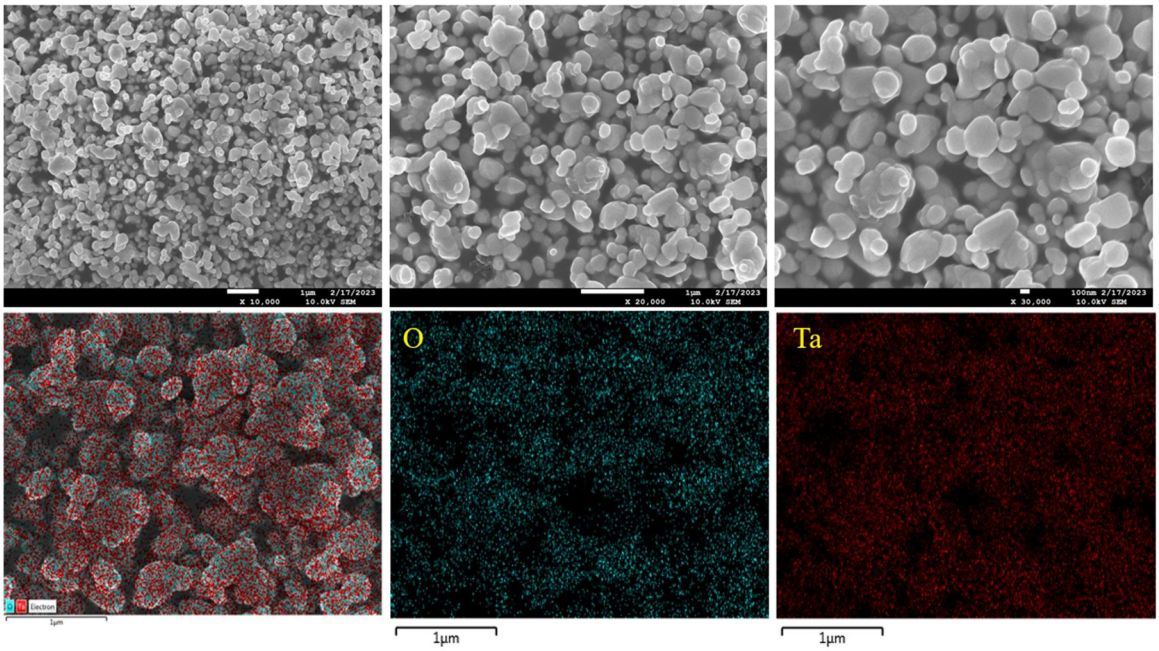

Figure 2.3. FE-SEM images and EDS mapping of $LiTaO_3$.

(b)

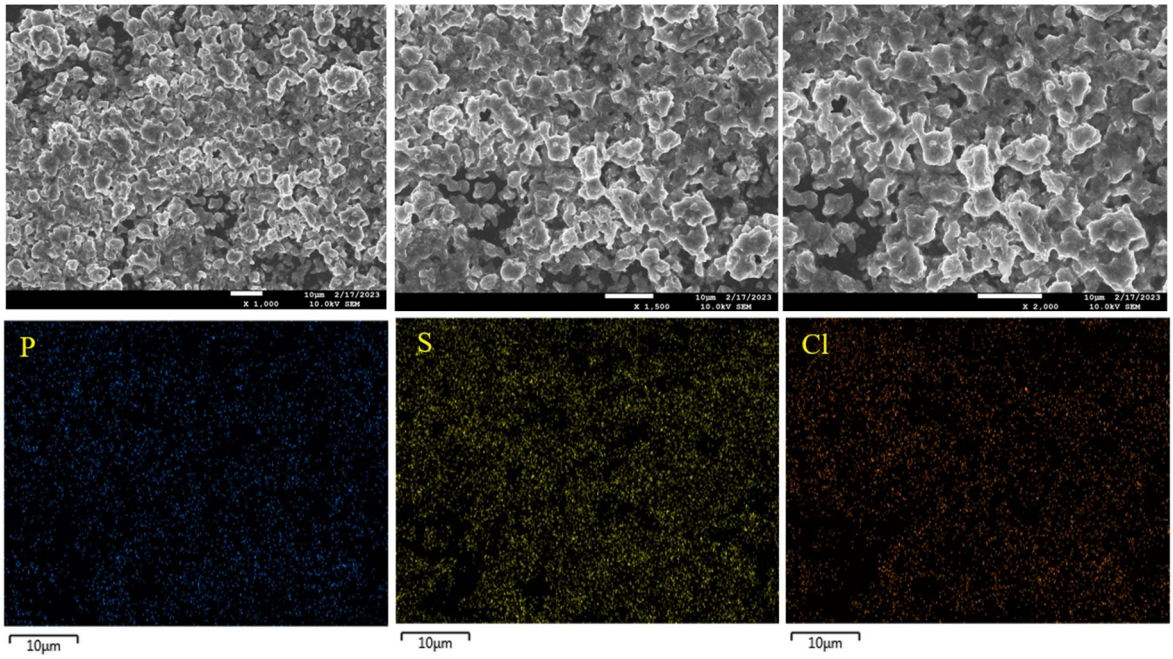

Figure 2.4. FE-SEM images and EDS mapping of $Li_{5.3}PS_{4.3}Cl_{1.7}$.

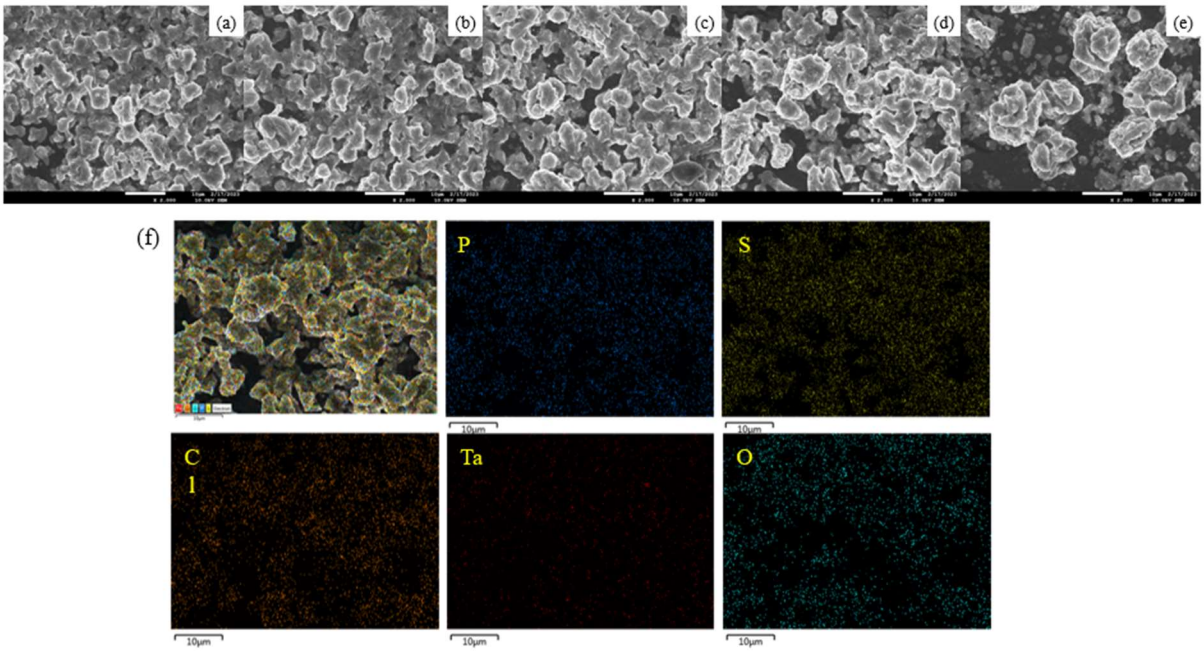

Figure 2.5. FE-SEM images of (a) pristine LPSCl, (b) 98LPSCl-2LTaO, (c) 96LPSCl-4LTaO, (d) 94LPSCl-6LTaO, (e) 92LPSCl-8LTaO, and (f) EDS analysis of 94LPSCl-6LTaO composition and their individual elemental mapping.

2-3-2. Electrochemical performance

Electrochemical Impedance Spectroscopy (EIS) was performed on all prepared solid electrolytes. The Nyquist plot of EIS performed at room temperature is shown in Figure 2.6. The ionic conductivity calculated from the measured resistance values is listed in Table 2.1, and the ionic conductivity is lower when $LiTaO_3$ is mixed than when pristine LPSCl is used (6.95mS/cm). This is because $LiTaO_3$, known to have an ionic conductivity of 10^{-7}S/cm, was simply mixed without changing the lattice structure [45]. 98LPSCl-2LTaO, 96LPSCl-4LTaO, and 94LPSCl-6LTaO have lower ionic conductivities than pristine LPSCl, but all three compositions show similar ionic conductivities (5.32~5.73mS/cm). 92LPSCl-8LTaO shows a sharply reduced ionic conductivity (4.29mS/cm). We believe that this is due to poor contact between the solid electrolytes due to agglomeration of particles in 92LPSCl-8LTaO.

In addition, temperature-dependent ionic conductivity analysis was performed on all solid electrolyte compositions to observe the activation energy according to $LiTaO_3$ mixing. The results are shown in Figure 2.7 and Table 2.2. The activation energy tendency of the solid electrolyte after mixing $LiTaO_3$ is similar to the ionic conductivity tendency. The activation energy of 98LPSCl-2LTaO, 96LPSCl-4LTaO, and 94LPSCl-6LTaO is slightly lower than that of pristine LPSCl, but is similar to each other, and the activation energy increases sharply in 92LPSCl-8LTaO. This seems to have contributed to the sharply reduced ionic conductivity. This is because mixing too much $LiTaO_3$ acts as a resistance.

A lower activation energy means that a lower potential energy barrier is required for ions to jump to adjacent lattice sites, resulting in more active lithium-ion jumps. Mixing $LiTaO_3$, which has relatively low ionic conductivity, with $Li_{5.3}PS_{4.3}Cl_{1.7}$, which has high ionic conductivity, is somewhat disadvantageous in terms of ionic conductivity and activation energy. However, this value is not unreasonable for application to batteries, and we focus on advances in the interface between the solid electrolyte and the cathode.

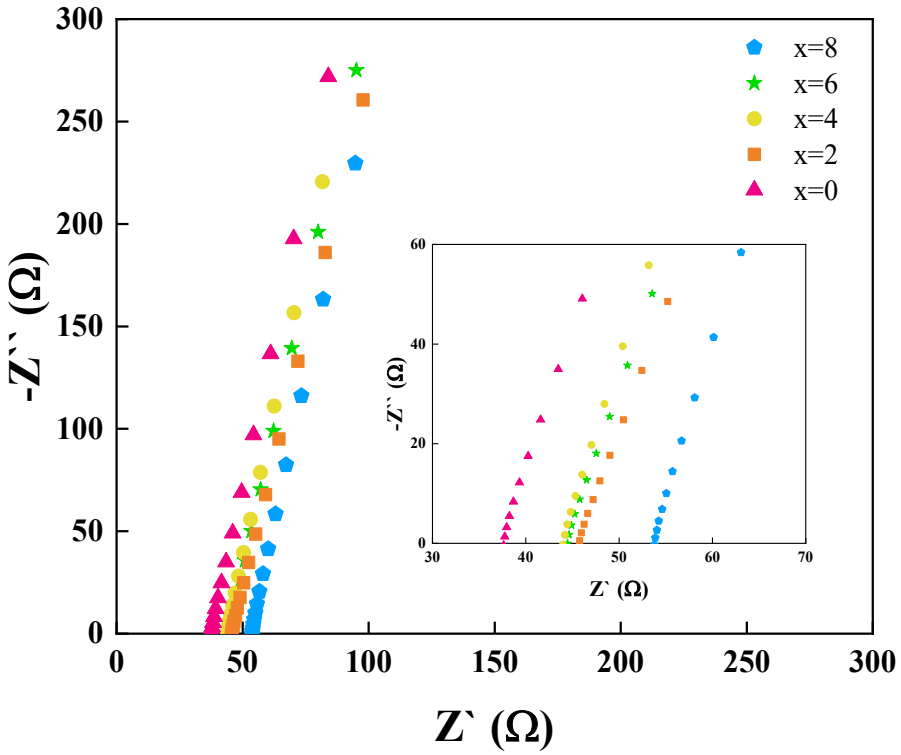

Figure 2.6. Nyquist plots of (100-x)$Li_{5.3}PS_{4.3}Cl_{1.7}$ – $xLiTaO_3$ (x=0, 2, 4, 6, and 8) solid electrolytes at room temperature.

Table 2.1. The ionic conductivity of the (100-x)$Li_{5.3}PS_{4.3}Cl_{1.7}$ – $xLiTaO_3$ (x=0, 2, 4, 6, and 8) at room temperature.

Solid electrolyte	Resistance (Ω)	Ionic conductivity (S cm^{-1})
$Li_{5.3}PS_{4.3}Cl_{1.7}$ (x = 0)	37.6	6.95 x 10^{-3}
98LPSCl-2LTaO (x = 2)	45.8	5.42 x 10^{-3}
96LPSCl-4LTaO (x = 4)	44.0	5.73 x 10^{-3}
94LPSCl-6LTaO (x = 6)	44.5	5.32 x 10^{-3}
92LPSCl-8LTaO (x = 8)	53.8	4.29 x 10^{-3}

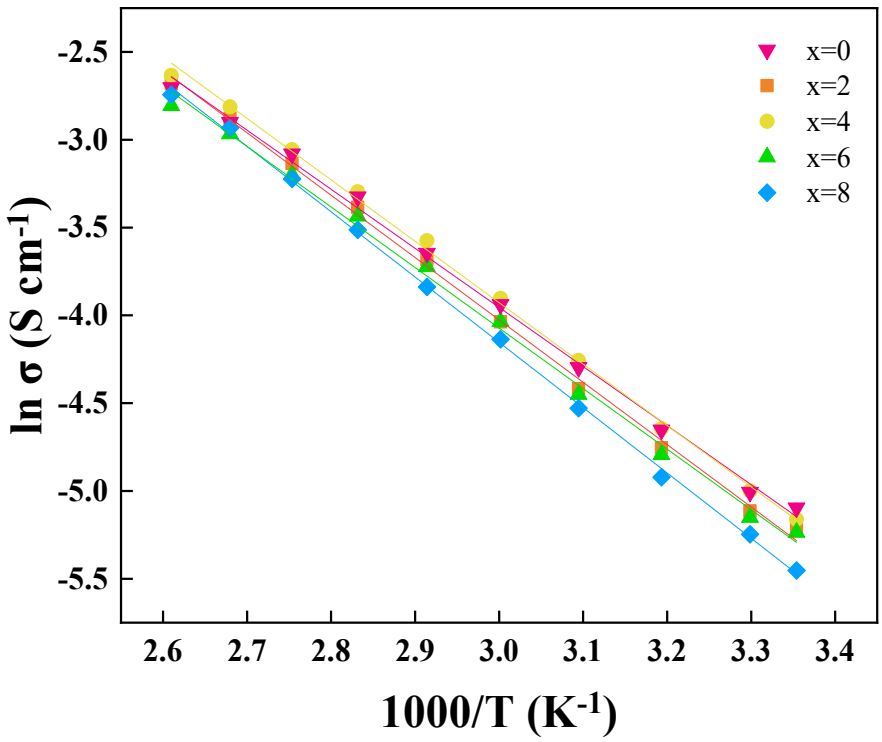

Figure 2.7. Arrhenius ionic conductivity plots from 298K to 383K of (100-x)$Li_{5.3}PS_{4.3}Cl_{1.7}$ – x$LiTaO_3$ (x=0, 2, 4, 6, and 8) solid electrolytes.

Table 2.2. The activation energy of the (100-x)$Li_{5.3}PS_{4.3}Cl_{1.7}$ – x$LiTaO_3$ (x=0, 2, 4, 6, and 8).

Solid electrolyte	Activation Energy(Ea)
$Li_{5.3}PS_{4.3}Cl_{1.7}$ (x = 0)	0.290 eV
98LPSCl-2LTaO (x = 2)	0.306 eV
96LPSCl-4LTaO (x = 4)	0.301 eV
94LPSCl-6LTaO (x = 6)	0.297 eV
92LPSCl-8LTaO (x = 8)	0.321 eV

Cyclic voltammetry (CV) was performed to evaluate the electrochemical stability window of the solid electrolyte. The CV data of the fabricated Li/SE/SUS asymmetric 2032 type coin cell is shown in Figure 2.8. For all compositions, the CV graph has a similar shape. As a result of investigating all samples from -0.5V to 5V (vs Li/Li^+), Peaks occurring due to lithium deposition ($Li^+ + e^- \rightarrow Li$) and dissolution ($Li \rightarrow Li^+ + e^-$) are observed around -0.5V and 0.5V. Afterwards, it shows stable electrochemical stability without any large side reaction peaks up to the 5V range.

When argygodite-based solid electrolyte is in direct contact with lithium, the interfacial reaction proceeds slowly but clearly [46]. In the CV graph of pristine LPSCl, the curve is not smooth even after 1V, but the solid electrolyte mixed with $LiTaO_3$ is smoother than pristine LPSCl. Additionally, as the mixing ratio of $LiTaO_3$ increases, the intensity of the redox peak generated by lithium tends to increase. It seems to be reasonable that mixing $LiTaO_3$ into the solid electrolyte helps improve electrochemical performance at the interface with lithium.

To investigate compatibility with lithium metal, a Li/SE/Li symmetric cell was assembled, and the critical current density was measured through DC cycling at 25°C. The data is shown in Figure 2.9. Among all solid electrolyte compositions, the x=4, 6 sample showed the highest critical current density of 0.65 mA/cm^2. At x=8, the critical current density rapidly decreases to 0.45mA/cm^2, which is lower than that of pristine LPSCl. This seems to be due to the rapidly reduced ionic conductivity and higher activation energy barrier in this composition. In this respect, electrochemical stability can be improved by mixing an appropriate amount of $LiTaO_3$, reducing the amount of irreversible lithium movement, and effectively increasing compatibility with Li metal.

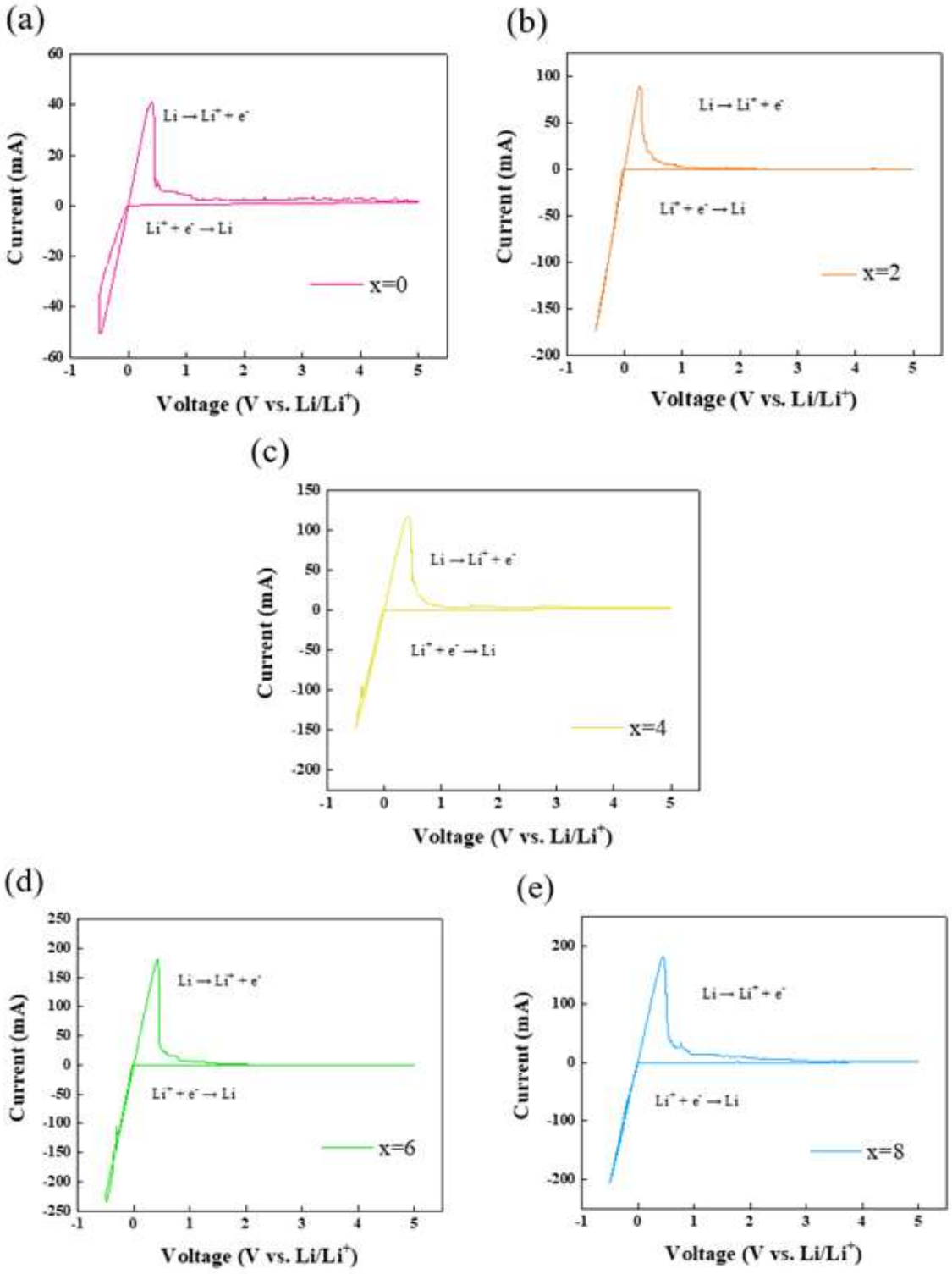

Figure 2.8. Cyclic voltammetry profiles of (a) pristine LPSCl, (b) 98LPSCl-2LTaO, (c) 96LPSCl-4LTaO, (d) 94LPSCl-6LTaO, and (e) 92LPSCl-8LTaO at a scan rate of 1 mV/s at room temperature.

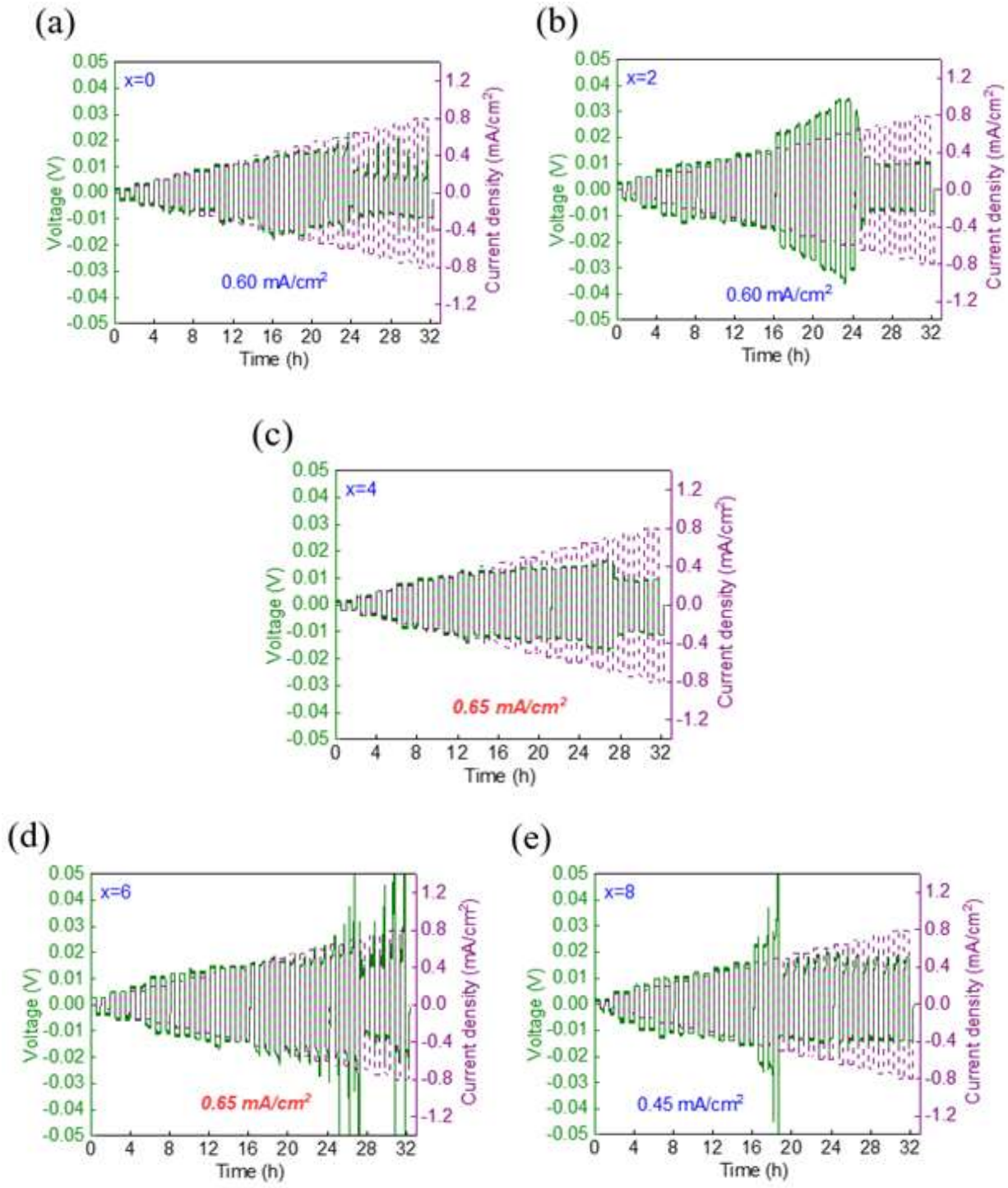

Figure 2.9. Critical current density confirmed through DC profile of (a) pristine LPSCl, (b) 98LPSCl-2LTaO, (c) 96LPSCl-4LTaO, (d) 94LPSCl-6LTaO, and (e) 92LPSCl-8LTaO at room temperature.

Here, we believed that the addition of $LiTaO_3$ could stabilize the interfacial stability between the cathode active material and the solid electrolyte during the charge and discharge process. To investigate the electrochemical performance of solid electrolyte samples, an ASSB was fabricated using composite as the cathode and Li as the anode material. The cathode composite for ASSB was a mixture of cathode active material (uncoated NCM811), conductive material (VGNF), and solid electrolyte. The initial charge/discharge curve and cycle stability of ASSBs manufactured using $(100\text{-}x)Li_{5.3}PS_{4.3}Cl_{1.7} - xLiTaO_3$ (x=0, 2, 4, 6, and 8) solid electrolytes are shown in Figure 2.10, and detailed cell performance values are listed in Table 2.3. ASSBs were operated at 0.1 c-rate in the 2.6-4.3V voltage range.

In the case of pristine LPSCl, the initial discharge capacity was measured at 159.1mAh/g, the coulombic efficiency was 69.47%, and the capacity retention up to the 50th cycle was 59.9%. The solid electrolyte mixed with $LiTaO_3$ showed higher initial discharge capacity, coulombic efficiency, and capacity retention than Pristine LPSCl in all cases. Until 94LPSCl-6LTaO, the more $LiTaO_3$ is mixed, the higher the battery performance is. 94LPSCl-6LTaO shows an initial discharge capacity of 174.4mAh/g, coulombic efficiency of 75.18%, and capacity retention of 74.4%, and shows the highest performance among all compositions.

However, the 92LPSCl-8LTaO solid electrolyte shows an initial discharge capacity of 164.4mAh/g, coulombic efficiency of 71.81%, and capacity retention of 71.2%, and battery performance deteriorates significantly. It seems that mixing $LiTaO_3$ stabilizes the interface between the cathode and the solid electrolyte, which leads to an increase in initial discharge capacity. This interface stabilization effect is appropriate up to x=6, but has the opposite effect at x=8. 92LPSCl-8LTaO solid electrolyte has low ionic conductivity and high activation energy due to increased resistance by agglomeration of particles and too large amounts of $LiTaO_3$. The decrease in discharge capacity is consistent with the rapid decrease in critical current density in DC profile.

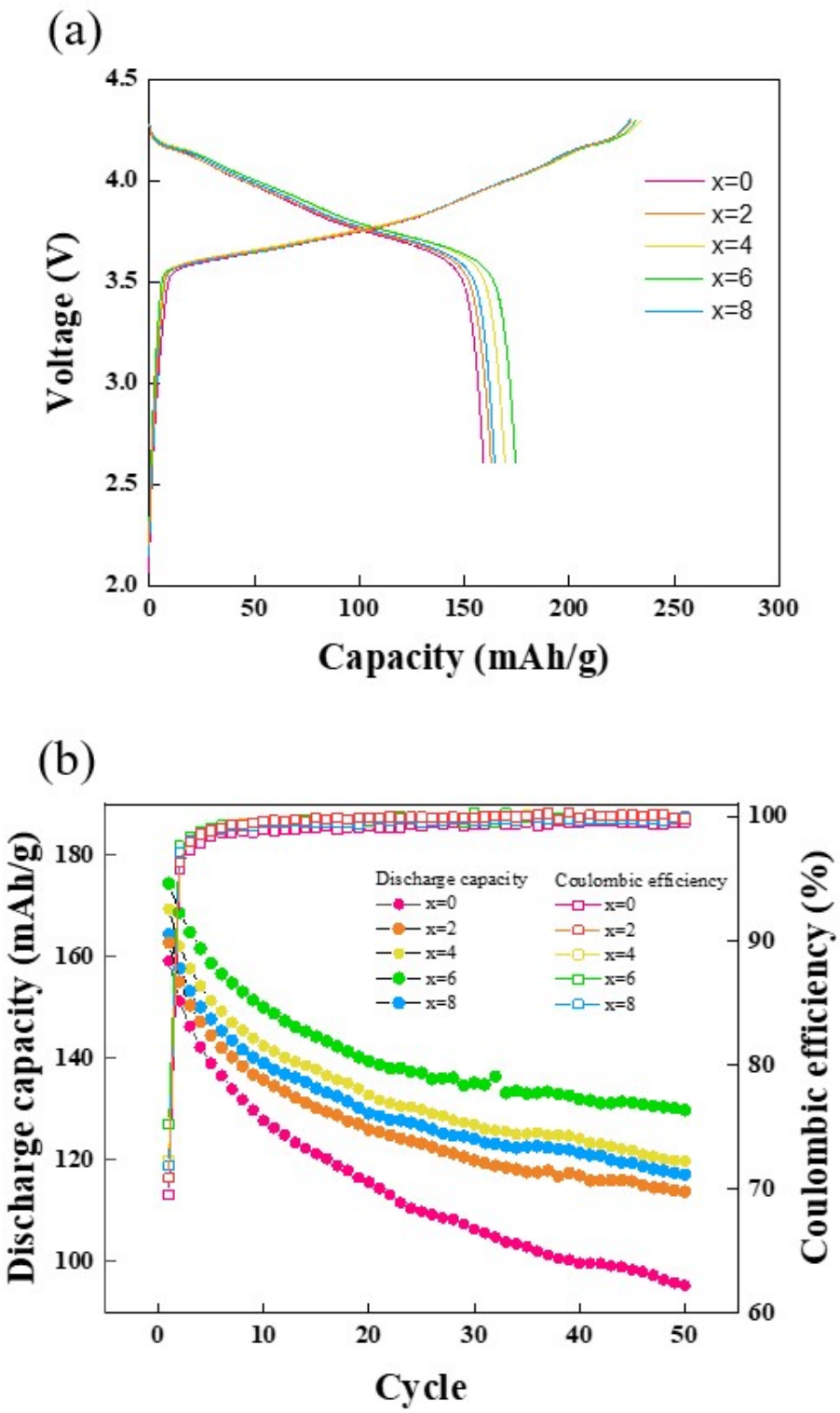

Figure 2.10. (a) First cycle of charge-discharge performance and (b) cycle stability of ASSBs fabricated using (100-x)$Li_{5.3}PS_{4.3}Cl_{1.7}$ – x$LiTaO_3$ (x=0, 2, 4, 6, and 8) solid electrolyte.

Table 2.3. Discharge capacity values, capacity retention and coulombic efficiency of ASSBs fabricated using (100-x)$Li_{5.3}PS_{4.3}Cl_{1.7}$ – x$LiTaO_3$ (x=0, 2, 4, 6, and 8) solid electrolyte.

	x=0	x=2	x=4	x=6	x=8
1^{st} cycle Discharge capacity (mAh/g)	159.1	162.7	169.3	174.4	164.4
11^{th} cycle Discharge capacity (mAh/g)	126.3	134.5	141.4	148.8	137.7
21^{th} cycle Discharge capacity (mAh/g)	114.4	125.4	131.7	138.8	128.7
31^{th} cycle Discharge capacity (mAh/g)	105.6	119.3	126.1	134.8	123.4
41^{th} cycle Discharge capacity (mAh/g)	99.7	115.9	123.4	131.7	120.9
50^{th} cycle Discharge capacity (mAh/g)	95.3	113.8	119.7	129.8	117.1
1^{st} – 50^{th} cycle retention (%)	59.9	69.9	70.7	74.4	71.2
Coulombic efficiency in 1^{st} cycle (%)	69.47	70.85	72.31	75.18	71.81

Therefore, we chose 94LPSCl-6LTaO as the solid electrolyte with the optimal composition. To elucidate the effect of $LiTaO_3$ mixing on electrochemical performance, four types of cells (Cell 1, 2, 3, and Ref) with different cathode composites and solid electrolytes were prepared, as shown in Figure 2.11. For all ASSBs made, Li was used as the anode.

The cathode composite used in Cell 1 was made by mixing uncoated NCM811, VGNF and LPSCl. LPSCl was applied to the solid electrolyte layer. So, Cell 1 is the same as the ASSB made with solid electrolyte of x=0 composition shown in Figure 2.10 and Table 2.3. The cathode composite used in Cell 3 was made by mixing uncoated NCM811, VGNF and LPSCl. 94LPSCl-6LTaO was applied to the solid electrolyte layer. So, Cell 3 is the same as ASSB made with solid electrolyte of x=6 composition shown in Figure 2.10 and Table 2.3.

The cathode composite used in Cell 2 was made by mixing uncoated NCM811, VGNF and 94LPSCl-6LTaO. Additionally, 94LPSCl-6LTaO was applied to the solid electrolyte layer. Cell 2 was produced to determine the effect when $LiTaO_3$ is not simply mixed in the solid electrolyte layer but also included in the cathode composite. The cathode composite used in Cell Ref was made by mixing $LiNbO_3$ coated NCM811, VGNF and LPSCl. LPSCl was applied to the solid electrolyte layer. Cell Ref does not use any $LiTaO_3$, and was created to compare the simple mixing of $LiTaO_3$ with the coating method (previously used to suppress side reactions between the cathode and the solid electrolyte).

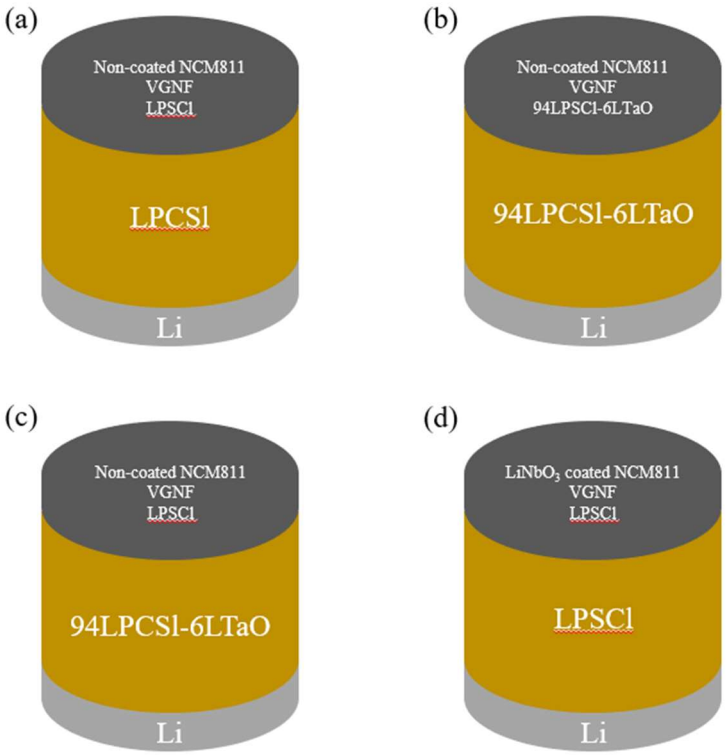

Figure 2.11. Schematic diagrams of (a) Cell 1, (b) Cell 2, (c) Cell 3, and (d) Cell Ref.

Figure 2.12 shows the cycle stability of the ASSB operated at 0.1 c-rate in the voltage range from 2.6-4.3 V (vs. Li/Li^+). Detailed data on this are given in Table 2.4. In the case of Cell 1 and Cell Ref, $LiTaO_3$ was not mixed at all. In the initial cycle, the discharge capacities of Cell 1 and Cell Ref were 159.1mAh/g and 156.6mAh/g, respectively, while the respective coulombic efficiencies were 69.47% and 73.74%. When $LiNbO_3$ is coated on the cathode active material, the initial discharge capacity decreases, but the coulombic efficiency increases. If charge movement occurs due to an unwanted side reaction at the interface between the electrode and the solid electrolyte in the first charge/discharge cycle, it can be expressed as an increase in charge capacity. In other words, the coulombic efficiency decreases. Therefore, the results can be interpreted to mean that the $LiNbO_3$ coating film contributes to reducing the degree of side reactions by covering the gap between the electrochemical stability windows of the solid electrolyte and NCM811. However, the $LiNbO_3$ coating film itself became a barrier to the movement of lithium ions, which caused the discharge capacity to decrease slightly.

In the case of Cell 3, $LiTaO_3$ was mixed only in the solid electrolyte layer. The initial discharge capacity was 174.4mAh/g, which was a significant increase compared to Cell 1 without any $LiTaO_3$ mixed in. It also showed a higher capacity retention rate and higher Coulombic efficiency than Cell 1. Therefore, mixing $LiTaO_3$, like coating $LiNbO_3$, stabilizes the interface between the cathode and the solid electrolyte.

In the case of Cell 2, $LiTaO_3$ was mixed not only in the solid electrolyte but also in the cathode composite. Compared to Cell 3, it can be observed from the results that the initial discharge capacity and retention rate are improved when $LiTaO_3$ is mixed into the cathode composite. Comparing Cell 2 and Cell Ref, Cell 2 has slightly higher Coulombic efficiency and clearly superior initial discharge capacity. Meanwhile, Cell Ref shows excellent performance in terms of capacity retention.

The method of both simply mixing $LiTaO_3$ into the solid electrolyte and coating $LiNbO_3$ on the cathode active material stabilizes the interface between the solid electrolyte and the cathode while also improving battery performance. Compared to the coating method, the simple mixing method is expected to be more conducive to the intercalation of lithium ions into the electrode structure. Comparing Cell 2 and Cell Ref, despite Cell 2's low retention rate, it shows a higher discharge capacity than Cell Ref, even at the 50th cycle, due to its high initial discharge capacity.

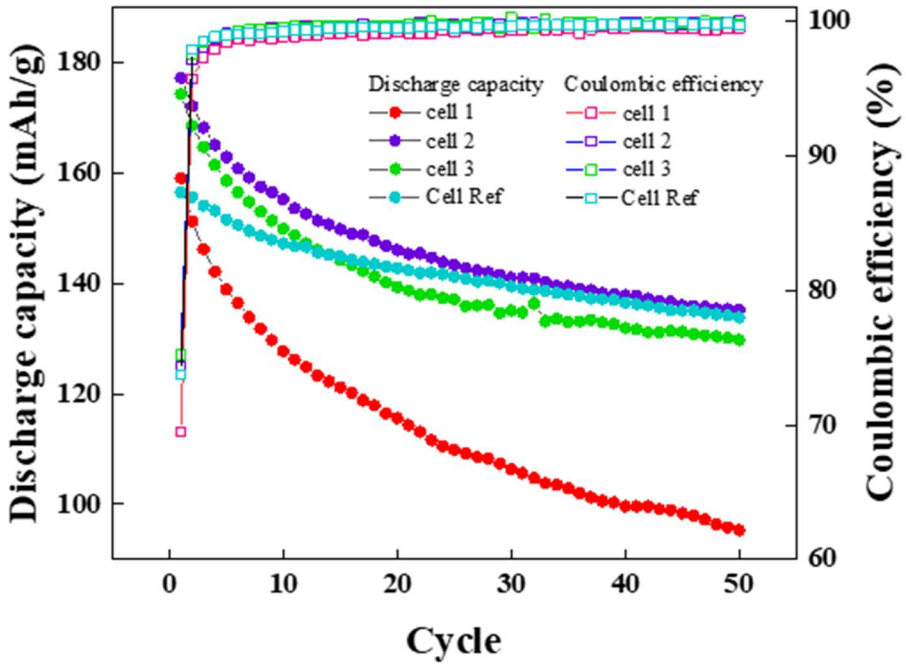

Figure 2.12. Cycle stability of Cell 1, 2, 3, and Ref.

Table 2.4. Discharge capacity values, capacity retentions, and Coulombic efficiencies of Cells 1, 2, 3, and Ref.

	Cell 1	Cell 2	Cell 3	Cell Ref
Solid electrolyte for cathode composite	LPSCl	94LPSCl-6LTaO	LPSCl	LPSCl
Solid electrolyte	LPSCl	94LPSCl-6LTaO	94LPSCl-6LTaO	LPSCl
Active material coating	-	-	-	$LiNbO_3$
1^{st} cycle discharge capacity (mAh/g)	159.1	177.3	174.4	156.6
21^{th} cycle discharge capacity (mAh/g)	114.4	145.4	138.8	142.4
50^{th} cycle discharge capacity (mAh/g)	95.3	135.3	129.8	133.9
1^{st} – 50^{th} cycle retention (%)	59.9	76.3	74.4	85.5
Coulombic efficiency in 1^{st} cycle (%)	69.47	74.31	75.18	73.74

Figure 2.13 shows the EIS spectra before and after charge/discharge tests for Cells 1, 2, and 3, which are ASSBs made of different cathode composites and solid electrolytes. Alternating current (AC) was applied in the frequency range of 7MHz to 0.01Hz at an amplitude of 50 mV. The equivalent circuits were used for fitting the ASSBs. Before cycling, the horizontal intercept in the high frequency region of the Nyquist plot is due to the bulk resistance (R1) of the solid electrolyte itself. Afterwards, the charge transferring resistance (R2), which appears as a Randles circuit, was included in the equivalent circuit and fitted. After cycling, an additional semicircle with a larger diameter appears. This is due to side reactions that occur during repeated charging and discharging. CEI (Cathode Electrolyte Interphase) layer resistance (R3) caused by side reactions was additionally applied to the equivalent circuit for fitting. Before cycling, as shown in Table 2.5, R1 was measured as 11.38Ω, 15.25Ω, and 15.11Ω for Cells 1, 2, and 3, respectively.

As mentioned in the previous section, pristine LPSCl has an ionic conductivity of 6.95mS/cm, which is about 1.3 times higher than the ionic conductivity of 94LPSCl-6LTaO, which is 5.32mS/cm. Cell 1, which uses a solid electrolyte with high ionic conductivity, shows the lowest R1 value, and Cell 2 and Cell 3, which use a solid electrolyte with low ionic conductivity, show higher R1 values. Since the same solid electrolyte was applied, the R1 values of Cell 2 and Cell 3 are similar. R2 is also due to the ionic conductivity of the solid electrolyte. R2 refers to the resistance in the process of transferring charge from the solid electrolyte layer to the electrode interface. The lowest resistance of R2 was measured in Cell 1 as 11.95Ω, which is the case without $LiTaO_3$ in both the solid electrolyte and the cathode composite.

In Cell 3, where $LiTaO_3$ was mixed only in the solid electrolyte layer, higher values of 17.60Ω were measured as R2. In the case of Cell 2, 94LPSCl-6LTaO, which has lower ionic conductivity, is mixed not only in the solid electrolyte but also in the cathode composite. The highest R2 value was measured at 19.70Ω. The resistance value of each cell after cycling is shown in Table 2.6. After repeated charging and discharging, the resistance of the layer created through side reactions was denoted as R3. The R3 values for Cells 1, 2, and 3 were measured to be 2797.4Ω, 1009.0Ω, and 1545.2Ω, respectively. These results are consistent with the trends in initial discharge capacity and retention rate shown by each ASSB. In other words, mixing $LiTaO_3$ in the solid electrolyte can stabilize the interface between the cathode and the solid

electrolyte, suppress side reactions, and ultimately lead to better battery performance. Moreover, when $LiTaO_3$ not only exists at the interface between the solid electrolyte and the cathode, but is also mixed inside the cathode active material itself, this interfacial stabilization effect becomes much greater, thereby more effectively suppressing the creation of layers due to side reactions.

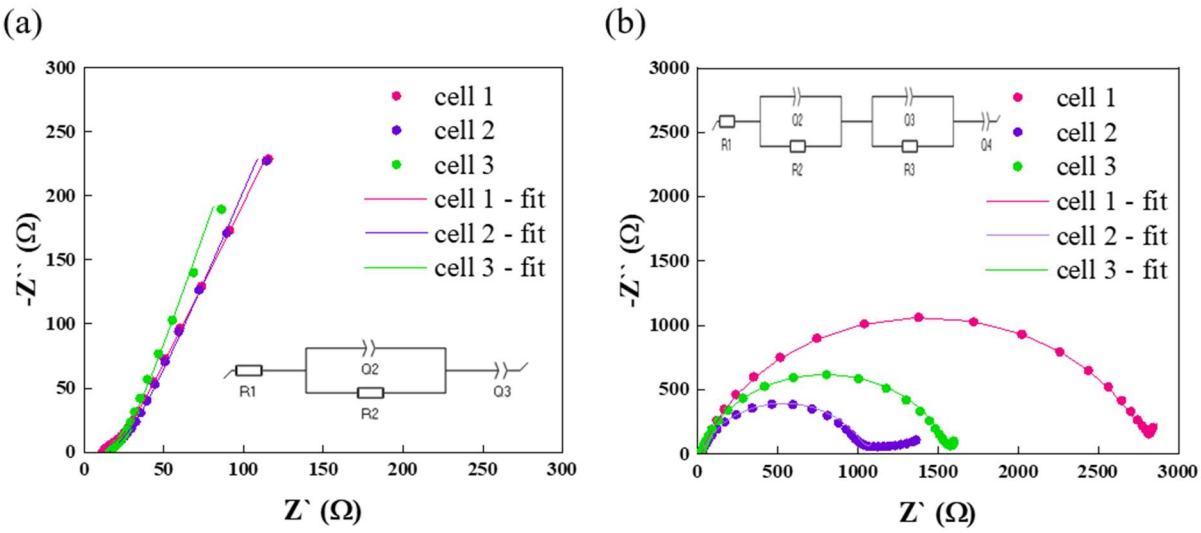

Figure 2.13. Nyquist plots of Cell 1, 2, and 3 (a) before and (b) after cycling.

Table 2.5. Impedance fitting data from the Cell 1, 2, and 3 before cycling.

	Cell 1	Cell 2	Cell 3
R1 (Ω)	11.38	15.25	15.11
R2 (Ω)	11.95	19.70	17.60

Table 2.6. Impedance fitting data from the Cell 1, 2, and 3 after cycling.

	Cell 1	Cell 2	Cell 3
R1 (Ω)	17.3	13.8	13.9
R2 (Ω)	4.1	11.54	6.1
R3 (Ω)	2797.4	1009.0	1545.2

2-3-3. Interfacial analysis

We measured XPS to analyze the interface between solid electrolyte and cathode. For this, coin cells that had been charged and discharged for up to 50 cycles were disassembled, and then cathode composite was collected. Figure 2.14 shows XPS graphs containing information about which element bonding exists on the surface at the interface. In Figure 2.14(a, c), the main peak (orange color) corresponding to PS_4^{3-} occurring in the region from 161.5 eV to 162.5 eV was observed. This peak appears because the solid electrolyte structurally has a PS_4^{3-} bond. The peak (sky color) that occurs at a higher bonding energy is due to S-S bonding and appears due to reduction and decomposition of the solid electrolyte. On the other hand, the peak (purple color) occurring at low bonding energy is caused by Li_2S transition metal sulfates and occurs as a side reaction at the interface between the solid electrolyte and the cathode. In Figure 2.14 (b, d), the peak due to PS_4^{3-} in the region from 131.5 eV to 132.5 eV is indicated in orange color. The peak (green color) occurring in the high binding energy region is caused by transition metal phosphates and appears due to a side reaction at the interface between the solid electrolyte and the cathode. The peak (yellow color) occurring in the lower bonding energy region is caused by reduced phosphorus species and is a peak generated by the reduction decomposition reaction of the solid electrolyte [38]. ASSB (Cell 2) containing $LiTaO_3$ in the solid electrolyte and cathode composite showed that the peak sum (light red) line in XPS corresponding to the S 2p component had a shoulder peak. This shows that deconvolution of the peak can reduce the peak intensity of other internal elements. Cell 2 has a clearly lower intensity of the purple peak than that of ASSB (Cell 1), which does not contain $LiTaO_3$. This suggests that the solid electrolyte-cathode side reaction caused by Li_2S transition metal sulfates was suppressed because of $LiTaO_3$. In Figure 2.14(b, d), comparing the XPS data corresponding to the P 2p component of Cell 1 and Cell 2, a large difference is observed in the raw peak (light gray color) line. When $LiTaO_3$ was not contained, the peak was very messy. This means that the interface between the solid electrolyte and the cathode is much more chemically/electrochemically unstable. Figure 2.14(d) shows that the intensity of the peaks caused by transition metal phosphates and the peaks caused by reduced phosphorus species are reduced. In other words, mixing $LiTaO_3$ with a solid electrolyte and cathode composite can improve the chemical/electrochemical stability at the interface, suppressing the reductive decomposition reaction of the solid electrolyte and reducing side reactions with the cathode.

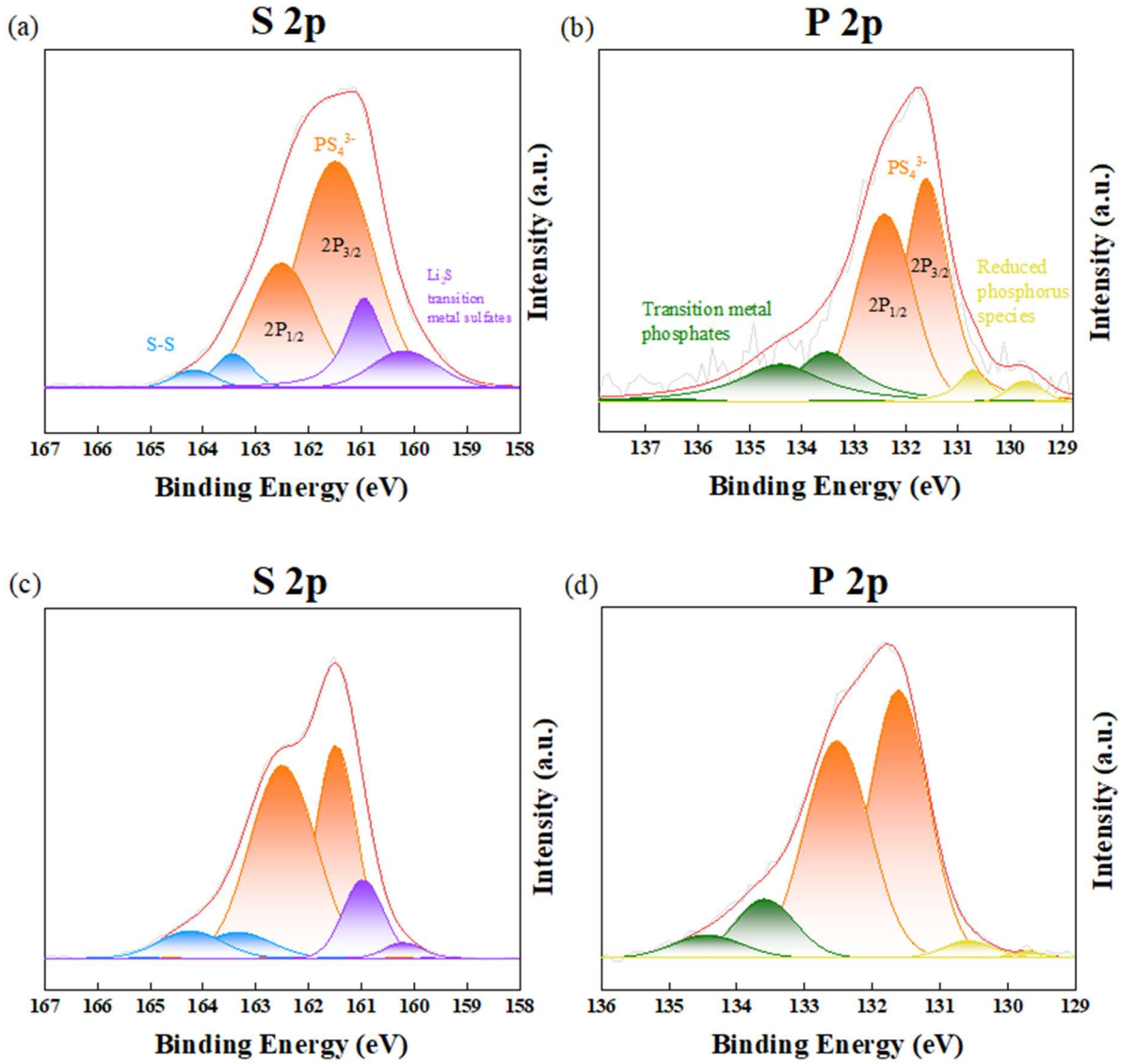

Figure 2.14. S 2p(a, c) and P 2p(b, d) XPS analysis on cathode composite of (a, b) Cell 1 and (c, d) Cell 2 after 50 cycles.

2-4. Conclusion

To improve the electrochemical performance of ASSB, LPSCl and $LiTaO_3$ were synthesized using a high-energy ball milling method and a wet milling method, respectively, and then simply mixed. It was confirmed through XRD that $LiTaO_3$ was simply mixed—and not doped—in the LPSCl solid electrolyte. After mixing $LiTaO_3$ with the LPSCl solid electrolyte, the ionic conductivity decreased slightly. The 94LPSCl-6LTaO solid electrolyte showed an ionic conductivity of 5.32mS/cm at room temperature, but it also showed a slight increase in critical current density to 0.65mA/cm^2. The electrochemical stability of solid electrolytes toward lithium metal was also studied through cyclic voltammetry and DC polarization techniques. Moreover, an ASSB made of non-coated NCM811/94LPSCl-6LTaO/Li was found to achieve excellent cycle performance with a higher specific capacity (174.4mAh/g) and retention (74.4%) than the corresponding values of an ASSB made of non-coated NCM811/LPSCl/Li. The ASSB made of 94LPSCl-6LTaO mixed non-coated NCM811/94LPSCl-6LTaO/Li achieved a specific capacity of 177.3mAh/g and a higher retention of 76.3%. The result of impedance analysis showed that, when $LiTaO_3$ was simply mixed in both the solid electrolyte layer and the cathode composite, the resistance due to CEI was measured as 1009.0Ω. This represented a decrease of about 64% compared to the case where $LiTaO_3$ was not mixed in at all, and a decrease of about 35% compared to the case where $LiTaO_3$ was mixed only in the solid electrolyte layer. These high specific capacity values and excellent cycling performance are attributed to the improved stability between the solid electrolyte and the cathode material during the electrochemical reaction.

2-5. References

[1] A. Sobianowska-Turek, W. Urbańska, A. Janicka, M. Zawiślak, J. Matla, The necessity of recycling of waste li-ion batteries used in electric vehicles as objects posing a threat to human health and the environment, Recycling. 6 (2021) 35.

[2] X. Zeng, M. Li, D. Abd El-Hady, W. Alshitari, A.S. Al-Bogami, J. Lu, K. Amine, Commercialization of lithium battery technologies for electric vehicles, Adv Energy Mater. 9 (2019) 1900161.

[3] G. Zubi, R. Dufo-López, M. Carvalho, G. Pasaoglu, The lithium-ion battery: State of the art and future perspectives, Renewable and Sustainable Energy Reviews. 89 (2018) 292–308.

[4] M. Li, C. Wang, Z. Chen, K. Xu, J. Lu, New concepts in electrolytes, Chem Rev. 120 (2020) 6783–6819.

[5] X. Shen, H. Liu, X.-B. Cheng, C. Yan, J.-Q. Huang, Beyond lithium ion batteries: Higher energy density battery systems based on lithium metal anodes, Energy Storage Mater. 12 (2018) 161–175.

[6] P.G. Balakrishnan, R. Ramesh, T.P. Kumar, Safety mechanisms in lithium-ion batteries, J Power Sources. 155 (2006) 401–414.

[7] J. Wen, Y. Yu, C. Chen, A review on lithium-ion batteries safety issues: existing problems and possible solutions, Materials Express. 2 (2012) 197–212.

[8] F. Zheng, M. Kotobuki, S. Song, M.O. Lai, L. Lu, Review on solid electrolytes for all-solid-state lithium-ion batteries, J Power Sources. 389 (2018) 198–213.

[9] Y.-K. Sun, Promising all-solid-state batteries for future electric vehicles, ACS Energy Lett. 5 (2020) 3221–3223.

[10] C. Sun, J. Liu, Y. Gong, D.P. Wilkinson, J. Zhang, Recent advances in all-solid-state rechargeable lithium batteries, Nano Energy. 33 (2017) 363–386.

[11] C. Wang, J. Liang, Y. Zhao, M. Zheng, X. Li, X. Sun, All-solid-state lithium batteries enabled by sulfide electrolytes: from fundamental research to practical engineering design, Energy Environ Sci. 14 (2021) 2577–2619.

[12] Z. Gao, H. Sun, L. Fu, F. Ye, Y. Zhang, W. Luo, Y. Huang, Promises, challenges, and recent progress of inorganic solid-state electrolytes for all-solid-state lithium batteries, Advanced Materials. 30 (2018) 1705702.

[13] Y. Seino, T. Ota, K. Takada, A. Hayashi, M. Tatsumisago, A sulphide lithium super ion conductor is superior to liquid ion conductors for use in rechargeable batteries, Energy Environ Sci. 7 (2014) 627–631.

[14] N. Kamaya, K. Homma, Y. Yamakawa, M. Hirayama, R. Kanno, M. Yonemura, T.

Kamiyama, Y. Kato, S. Hama, K. Kawamoto, A. Mitsui, A lithium superionic conductor, Nat Mater. 10 (2011) 682–686.

[15] X. Bai, Y. Duan, W. Zhuang, R. Yang, J. Wang, Research progress in Li-argyrodite-based solid-state electrolytes, Journal of Materials Chemistry A. 8 (2020) 25663–25686.

[16] M. Ghidiu, J. Ruhl, S.P. Culver, W.G. Zeier, Solution-based synthesis of lithium thiophosphate superionic conductors for solid-state batteries: A chemistry perspective, Journal of Materials Chemistry A. 7 (2019) 17735–17753.

[17] M.A. Kraft, S.P. Culver, M. Calderon, F. Böcher, T. Krauskopf, A. Senyshyn, C. Dietrich, A. Zevalkink, J. Janek, W.G. Zeier, Influence of lattice polarizability on the ionic conductivity in the lithium superionic argyrodites Li_6PS_5X (X= Cl, Br, I), J Am Chem Soc. 139 (2017) 10909–10918.

[18] P. Adeli, J.D. Bazak, K.H. Park, I. Kochetkov, A. Huq, G.R. Goward, L.F. Nazar, Boosting solid-state diffusivity and conductivity in lithium superionic argyrodites by halide substitution, Angewandte Chemie International Edition. 58 (2019) 8681–8686.

[19] C. Yu, Y. Li, M. Willans, Y. Zhao, K.R. Adair, F. Zhao, W. Li, S. Deng, J. Liang, M.N. Banis, R.Li, H. Huang, L. Zhang, R. Yang, S. Lu, Y. Huang, X. Sun, Superionic conductivity in lithium argyrodite solid-state electrolyte by controlled Cl-doping, Nano Energy. 69 (2020) 104396.

[20] Y. Xiao, L.J. Miara, Y. Wang, G. Ceder, Computational screening of cathode coatings for solid-state batteries, Joule. 3 (2019) 1252–1275.

[21] G.F. Dewald, S. Ohno, M.A. Kraft, R. Koerver, P. Till, N.M. Vargas-Barbosa, J. Janek, W.G. Zeier, Experimental assessment of the practical oxidative stability of lithium thiophosphate solid electrolytes, Chemistry of Materials. 31 (2019) 8328–8337.

[22] T.-T. Zuo, R. Rueß, R. Pan, F. Walther, M. Rohnke, S. Hori, R. Kanno, D. Schröder, J. Janek, A mechanistic investigation of the $Li_{10}GeP_2S_{12}$| $LiNi_{1-x-y}Co_xMn_yO_2$ interface stability in all-solid-state lithium batteries, Nat Commun. 12 (2021) 6669.

[23] S. Deng, X. Li, Z. Ren, W. Li, J. Luo, J. Liang, J. Liang, M.N. Banis, M. Li, Y. Zhao, X. Li, C. Wang, Y. Sun, Q. Sun, R. Li, Y. Hu, H. Huang, L. Zhang, S. Lu, J. Luo, X. Sun, Dual-functional interfaces for highly stable Ni-rich layered cathodes in sulfide all-solid-state batteries, Energy Storage Mater. 27 (2020) 117–123.

[24] M. Du, K. Liao, Q. Lu, Z. Shao, Recent advances in the interface engineering of solid-state Li-ion batteries with artificial buffer layers: challenges, materials, construction, and characterization, Energy Environ Sci. 12 (2019) 1780–1804.

[25] X. Li, Q. Sun, Z. Wang, D. Song, H. Zhang, X. Shi, C. Li, L. Zhang, L. Zhu, Outstanding electrochemical performances of the all-solid-state lithium battery using Ni-rich layered oxide cathode and sulfide electrolyte, J Power Sources. 456 (2020) 227997.

[26] H.W. Kwak, Y.J. Park, Li_2MoO_4 coated Ni-rich cathode for all-solid-state batteries, Thin

Solid Films. 660 (2018) 625–630.

[27] D.H. Yoon, Y.J. Park, Electrochemical Properties of Cathode According to the Type of Sulfide Electrolyte and the Application of Surface Coating, Journal of Electrochemical Science and Technology. 12 (2021) 126–136.

[28] S.H. Jung, K. Oh, Y.J. Nam, D.Y. Oh, P. Brüner, K. Kang, Y.S. Jung, Li_3BO_3–Li_2CO_3: rationally designed buffering phase for sulfide all-solid-state Li-ion batteries, Chemistry of Materials. 30 (2018) 8190–8200.

[29] F. Walther, F. Strauss, X. Wu, B. Mogwitz, J. Hertle, J. Sann, M. Rohnke, T. Brezesinski, J. Janek, The working principle of a Li_2CO_3/$LiNbO_3$ coating on NCM for thiophosphate-based all-solid-state batteries, Chemistry of Materials. 33 (2021) 2110–2125.

[30] N. Ohta, K. Takada, I. Sakaguchi, L. Zhang, R. Ma, K. Fukuda, M. Osada, T. Sasaki, $LiNbO_3$-coated $LiCoO_2$ as cathode material for all solid-state lithium secondary batteries, Electrochem Commun. 9 (2007) 1486–1490.

[31] X. Li, L. Jin, D. Song, H. Zhang, X. Shi, Z. Wang, L. Zhang, L. Zhu, $LiNbO_3$-coated $LiNi_{0.8}Co_{0.1}Mn_{0.1}O_2$ cathode with high discharge capacity and rate performance for all-solid-state lithium battery, Journal of Energy Chemistry. 40 (2020) 39–45.

[32] G. Lu, X. Li, Z. Wang, D. Song, H. Zhang, C. Li, L. Zhang, L. Zhu, Enhanced electrochemical performances of $LiCoO_2$ cathode for all-solid-state lithium batteries by regulating crystallinity and composition of coating layer, J Power Sources. 468 (2020) 228372.

[33] S. Ito, S. Fujiki, T. Yamada, Y. Aihara, Y. Park, T.Y. Kim, S.-W. Baek, J.-M. Lee, S. Doo, N. Machida, A rocking chair type all-solid-state lithium ion battery adopting Li_2O–ZrO_2 coated $LiNi_{0.8}Co_{0.15}Al_{0.05}O_2$ and a sulfide based electrolyte, J Power Sources. 248 (2014) 943–950.

[34] Y.G. Lee, S. Fujiki, C.H. Jung, N. Suzuki, N. Yashiro, R. Omoda, D.S. Ko, T. Shiratsuchi, T. Sugimoto, S.B. Ryu, J.H. Ku, T. Watanabe, Y.S. Park, Y. Aihara, D.M. Im, I.T. Han, High-energy long-cycling all-solid-state lithium metal batteries enabled by silver–carbon composite anodes, Nat Energy. 5 (2020) 299–308.

[35] J.S. Lee, Y.J. Park, Surface Modification of Cathode Via Precursor Coating for All-Solid-State Batteries, Electrochemical Society Meeting Abstracts, MA2020-02 (2020) 930.

[36] C.B. Lim, Y.J. Park, Precursor-based surface modification of cathodes using Ta and W for sulfide-based all-solid-state batteries, Sci Rep. 10 (2020) 10501.

[37] J.S. Lee, Y.J. Park, Comparison of $LiTaO_3$ and $LiNbO_3$ surface layers prepared by post- and precursor-based coating methods for Ni-rich cathodes of all-solid-state batteries, ACS Appl Mater Interfaces. 13 (2021) 38333–38345.

[38] J.U. Cho, R. Rajagopal, D.H. Yoon, Y.J. Park, K.S. Ryu, Control of side reactions using

$LiNbO_3$ mixed/doped solid electrolyte for enhanced sulfide-based all-solid-state batteries, Chemical Engineering Journal. 452 (2023) 138955.

[39] Y. Subramanian, R. Rajagopal, K.S. Ryu, Blending a Li_3N/Li_3YCl_6 solid electrolyte with Li_6PS_5Cl argyrodite structure to improve interface stability and electrochemical performance in Lithium solid-state batteries, J Alloys Compd. 940 (2023) 168867.

[40] C. Bi-Shiou, T.Y. Lin, D. Jenq-Gong, Sintering behavior and dielectric characteristics of $LiTaO_3$ with the addition of (Mg_2 + TiO_2), Mater Chem Phys. 28 (1991) 51–68.

[41] W. Huang, L. Cheng, S. Hori, K. Suzuki, M. Yonemura, M. Hirayama, R. Kanno, Ionic conduction mechanism of a lithium superionic argyrodite in the Li–Al–Si–S–O system, Mater Adv. 1 (2020) 334–340.

[42] S. V Patel, S. Banerjee, H. Liu, P. Wang, P.-H. Chien, X. Feng, J. Liu, S.P. Ong, Y.-Y. Hu, Tunable Lithium-Ion Transport in Mixed-Halide Argyrodites $Li_{6-x}PS_{5-x}ClBr_x$: An Unusual Compositional Space, Chemistry of Materials. 33 (2021) 1435–1443.

[43] D.A. Ziolkowska, W. Arnold, T. Druffel, M. Sunkara, H. Wang, Rapid and economic synthesis of a Li_7PS_6 solid electrolyte from a liquid approach, ACS Appl Mater Interfaces. 11 (2019) 6015–6021.

[44] Y. Zhu, S. Lin, Y. Liu, D. Ma, B. Wang, Efficient synthesis of stoichiometric lithium tantalate powder by a solid-state combustion route, Materials and Manufacturing Processes. 30 (2015) 1342–1347.

[45] N. Kamarulzaman, L. Widarti Zainudin, R. Yahaya Subban, Z. Osman, Comparison of Ionic Diffusion in Sol-Gel derived Micron and Nano $LiTaO_3$, Defect and Diffusion Forum. 312-315 (2011) 1222-1227.

[46] S. Wenzel, S.J. Sedlmaier, C. Dietrich, W.G. Zeier, J. Janek, Interfacial reactivity and interphase growth of argyrodite solid electrolytes at lithium metal electrodes, Solid State Ion. 318 (2018) 102–112.

Chapter 3. The improvement of electrochemical performance by mixing InF_3 in $Li_{5.3}PS_{4.3}Cl_{1.7}$ solid electrolyte

3-1. Introduction

Conventional lithium secondary batteries have made use of liquid electrolytes. All-solid-state batteries (ASSB), attracting attention as next-generation batteries, replace liquid electrolytes with solid electrolytes and have high energy density and high safety. In addition, as expected it is currently receiving much attention in electric vehicles [1–4]. The disadvantage of solid electrolytes was their low ionic conductivity. However, new compositions or methods such as doping, have achieved high ionic conductivity comparable to liquid electrolytes at room temperature. Another problem with solid electrolytes is the stability of the interface with the electrode [5]. The solid electrolyte can also act as a separator and has higher mechanical strength than existing polymer separators. Therefore, there have been attempts to apply lithium metal as an anode [6–8].

Since lithium, metal has a small atomic weight and a shallow standard electrode potential, when applied as an anode in a battery, the specific capacity is very high at about 3860mAh/g, and high energy density can be obtained [9]. However, the lithium metal grows into irreversible dendrites with repeated charging and discharging, causing internal short circuits and battery stability problems. Additionally, a side reaction occurs when the solid electrolyte reduces through lithium. As SEI (Solid Electrolyte Interphase) is created, the resistance at the interface gradually increases, deteriorating battery performance [10]. Even in the case of Li_6PS_5Cl, a sulfide-based solid electrolyte that is relatively chemically/ electrochemically stable and has high ionic conductivity, the interfacial reaction proceeds slowly and clearly when in direct contact with a lithium anode [11].

Meanwhile, indium is a metal that easily forms an alloy with lithium, and the redox level of the alloy formation reaction is 0.6V. Therefore, using indium metal as an anode can suppress battery performance degradation by reducing the thermodynamic driving force that causes a reduction of the sulfide solid electrolyte [12, 13]. Another way to stabilize the interface between

lithium and solid electrolyte is to create an interphase at the interface. Materials that can cover both the electrochemical stability window of lithium and solid electrolyte should chose as an interphase, and have a wide band gap and low electronic conductivity. If a material with high electronic conductivity forms as an interphase, the reduction/decomposition reaction of the solid electrolyte continues, causing the SEI layer to become thicker and the battery performance to deteriorate [14]. LiF crystal material has some fascinating physical properties such as high mechanical strength, low solubility, wide band gap (effectively prevents electron tunneling), and a high voltage window (up to 6.4 V vs Li/Li^+), all of which suggest that LiF can be used as a suitable component for SEI [15–17].

In this study, we attempt to stabilize the lithium anode interface by mixing InF_3 with $LI_{5.3}PS_{4.3}Cl_{1.7}$ sulfide-based solid electrolyte. InF_3 is expected to react with Li anode to create artificial SEI made of LiF and Li-In alloy [15]. To synthesize the solid electrolyte $Li_{5.3}PS_{4.3}Cl_{1.7}$, high-energy ball milling utilized. Hand grinding was performed to simply mix InF_3 with the solid electrolyte. Powder X-ray diffraction (XRD) was used to confirm the composition of InF_3. The ionic conductivity of the optimized composition was 5.46mS/cm at room temperature. The optimized electrolyte showed a high initial discharge capacity of 172.8mAh/g and excellent retention.

3-2. Experimental

3-2-1. Preparation of $Li_{5.3}PS_{4.3}Cl_{1.7}$ mixed xwt% InF_3 (x = 0, 1, 2, 3, and 4)

Li_2S (99.98%, Sigma), P_2S_5 (99%, Sigma) and LiCl (99.9%, Sigma) were used as a starting precursor to synthesize $Li_{5.3}PS_{4.3}Cl_{1.7}$. The above precursors weigh the stoichiometric ratio of the $Li_{5.3}PS_{4.3}Cl_{1.7}$ and grind uniformly using a hand-grinding process for 30 minutes in an argon atmosphere. Afterwards, the mixed powder is transferred to a zirconium jar, sealed, and subjected to high-energy ball milling at a speed of 500 rpm for 8 hours. After ball milling, the powder is pelletized at 20kN and sintered at 500℃ for 15 hours with an increasing heating rate of 2℃ min^{-1}, followed by hand grinding for 30 minutes to obtain the final solid electrolyte. $Li_{5.3}PS_{4.3}Cl_{1.7}$ and InF_3 are mixed through simple hand grinding for 15 minutes. InF_3 was mixed in the solid electrolyte at a ratio of 1, 2, 3, and 4wt%. To comparison, we also prepared $Li_{5.3}PS_{4.3}Cl_{1.7}$ without InF_3. Synthesized pristine solid electrolyte, $Li_{5.3}PS_{4.3}Cl_{1.7}$ named as LPSCl, and solid electrolytes prepared by mixing InF_3 named in the order as 99LPSCl-1InF, 98LPSCl-2InF, 97LPSCl-3InF and 96LPSCl-4InF.

3-2-2. Characterization and electrochemical performance measurements

Electrochemical Impedance Spectroscopy (EIS) determines the synthesized solid electrolyte's ionic conductivity and analyzes the resistance factor of ASSB. To determine the ionic conductivity of the synthesized solid electrolyte, Solid electrolyte powder (250 mg) was placed in a mold with a diameter of 10 mm and pressed at 20kN to pelletize it. Indium foil was attached to both sides of the pellet to create an In/SE/In symmetrical cell. We used Biologic (Sp-300) to apply alternating current (AC) at amplitude of 50mV in the frequency range of 7MHz to 1Hz, and ionic conductivity at room temperature (RT) using this method. Additionally, we measured EIS by applying the same process from 30°C to 110°C at 10°C intervals to obtain activation energy.

Cyclic voltammetry (CV) determines the electrochemical stability window of the solid electrolyte. To create the Li/SE/SUS asymmetric 2032-type coin cell, a mold with a 16mm diameter was filled with 200mg of Solid electrolyte powder. At room temperature, the cell was

scanned at a rate of 1 mV/s, starting from –0.5 V to 5.0 V. The experiment used a potentiostat/ galvanostatic system (SP-300, BioLogic).

ASSB was made using the synthesized solid electrolyte, and charge/discharge performance was tested. Using a vortex mixer, the cathode composite was prepared by mixing uncoated NCM811: solid electrolyte: VGNF = 70: 27: 3 ratio. During the assembly process, solid electrolyte powder (200 mg) was placed in a 16 mm diameter mold and pressed at 40kN to pelletize. Then, 5.5 mg of cathode composite disperses evenly on the surface of the solid electrolyte pellet. Afterward, put indium foil, spacer, and press with 40kN, then put Li and spacer on the other side and press with 7kN. The last step involved assembling the pellet inside a coin cell of the 2032 type. The charge-discharge cycling tests were analyzed at voltage ranges from 2.6-4.3 V (vs. Li/Li^+) with a current rate of 0.1C at 25℃ using the WonAtech WBCS 3000 battery test equipment.

3-3. Results and discussion

3-3-1. Structural characterization of InF_3 mixed $Li_{5.3}PS_{4.3}Cl_{1.7}$ solid electrolyte

X-ray diffraction (XRD) confirms the solid electrolyte and the mixing of InF_3 into the solid electrolyte. Figure 3.1 shows the XRD pattern of synthesized $Li_{5.3}PS_{4.3}Cl_{1.7}$ mixed xwt% InF_3 (x = 0, 1, 2, 3, and 4). Solid electrolytes of all compositions exhibit an argyrodite-type crystalline phase of cubic phase Li_7PS_6 (JCPDS-34-0688) with space group $\bar{F}43m$ [18–20]. The prominent diffraction peaks at 2θ = 15.4°, 17.8°, 25.4°, 29.8°, 31.2°, 39.7°, 44.9°, 47.7°, and 52.3° can be indexed to (111), (200), (220), (311), (222), (331), (422), (511), and (440) planes, respectively. The introduction of InF_3 in the solid electrolyte did not cause any change in the argyrodite structure, as shown in the XRD graph. When InF_3 mixes to x=1, the prominent peak of InF_3 appears separately from the peak corresponding to the argyrodite structure. Even if the mole fraction of InF_3 increases, only the peak intensity of InF_3 increases. This indicates that InF_3 was not doped into the structure, resulting in a simple mixing effect.

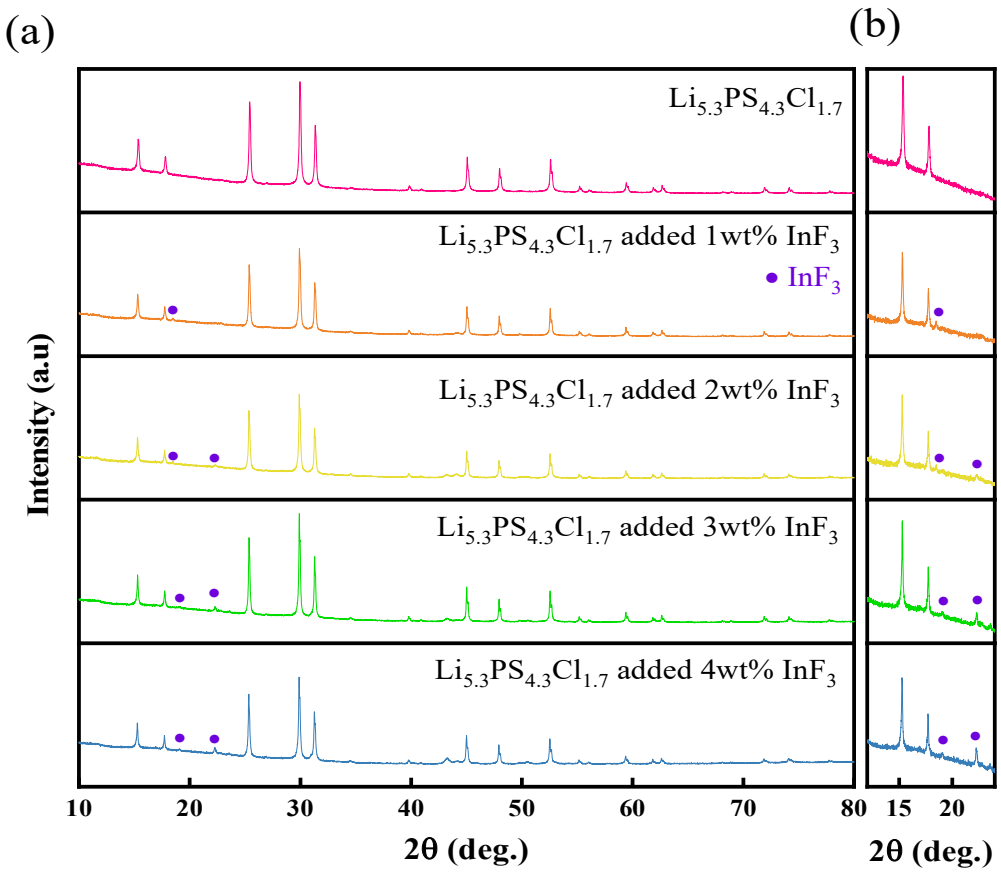

Figure 3.1. (a) Powder X-ray diffraction patterns of $Li_{5.3}PS_{4.3}Cl_{1.7}$ mixed xwt% InF_3 (x = 0, 1, 2, 3, and 4) solid electrolytes and (b) XRD with enlarged InF_3 peak area.

Figure 3.2 shows the FE-SEM images and elemental distribution of the synthesized solid electrolytes by EDS analysis. The particle shape of $Li_{5.3}PS_{4.3}Cl_{1.7}$ is irregular and the size ranges from 1 to several micrometers. EDS analysis of each solid electrolyte confirmed that each element distributes evenly within the particles. The consistent distribution patterns of P, S, Cl, In, and F elements support the solid electrolyte was well synthesized. As additional grinding was performed for InF_3 mixing, which confirms that the particles were broken and separated compared to pristine LPSCl. It confirms that there was no particle size or morphology change as the amount of InF_3 mixing increased.

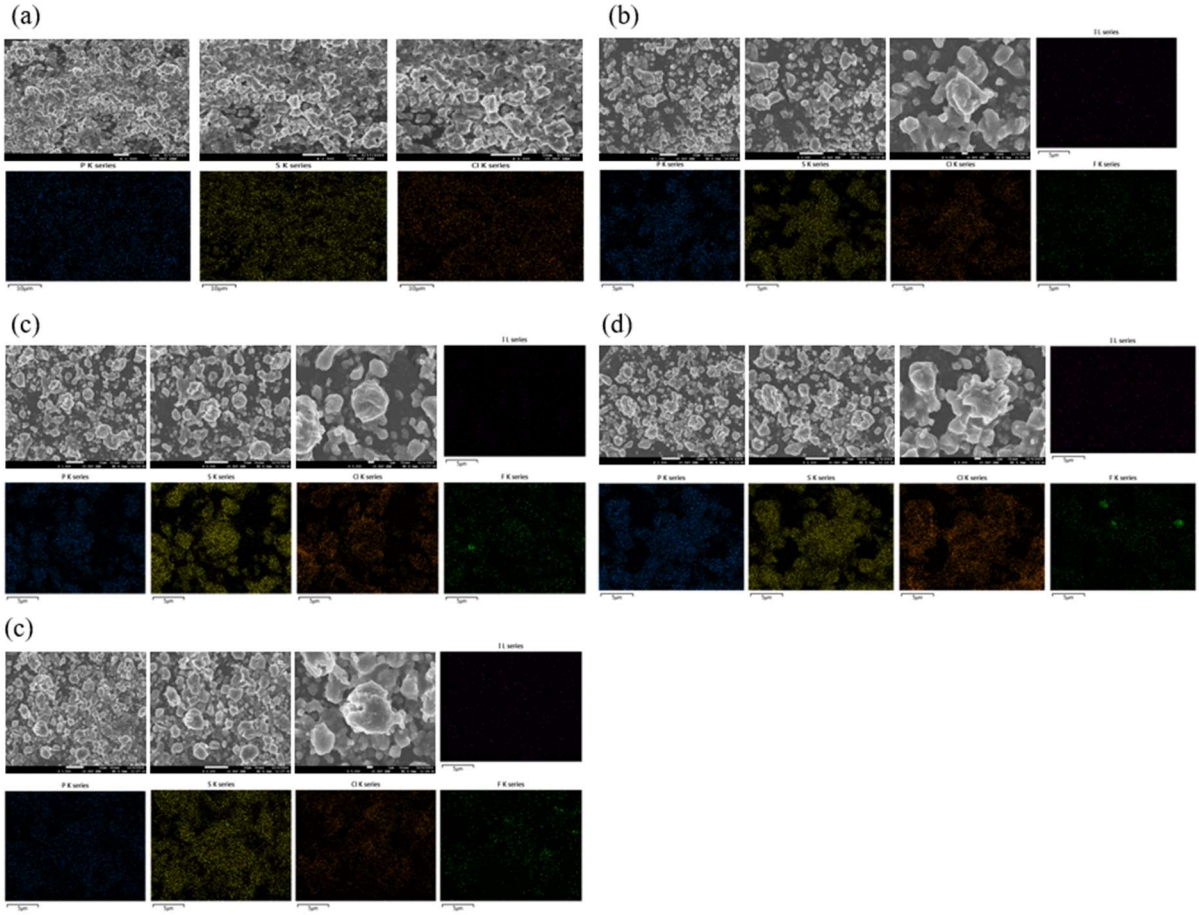

Figure 3.2. FE-SEM images and EDS mappings of (a) pristine LPSCl, (b) 99LPSCl-1InF, (c) 98LPSCl-2InF, (d) 97LPSCl-3InF, and (e) 96LPSCl-4InF.

3-3-2. Electrochemical performance

Electrochemical Impedance Spectroscopy (EIS) was performed on the prepared solid electrolytes. The Nyquist plot of EIS performed at room temperature is shown in Figure 3.3(a), and the ionic conductivity calculated from the measured resistance values is shown in Figure 3.3(b). The ionic conductivity is lower when InF_3 is mixed than when pristine LPSCl is used (6.66mS/cm). This is because InF_3 has lower ionic conductivity than the solid electrolyte, thus acting as a resistance. The ionic conductivity decreases as the InF_3 includes the solid electrolyte more.

In addition, temperature-dependent analysis on ionic conductivity was performed for all solid electrolyte compositions to observe the activation energy according to InF_3 mixing. Figure 3.4 shows the results. As InF_3 is mixed, the activation energy of the solid electrolyte gradually increases. This is the same as the tendency of ionic conductivity, and it is also because the ionic conductivity of InF_3 itself is relatively lower than that of the solid electrolyte.

Lower activation energy means a lower potential energy barrier is required for ions to jump to adjacent lattice sites, resulting in more active lithium-ion jumps. Mixing InF_3 is disadvantageous in terms of ionic conductivity and activation energy. However, this value is not unreasonable for application to batteries, and we focus on advances in the interface between the solid electrolyte and the Li-metal anode.

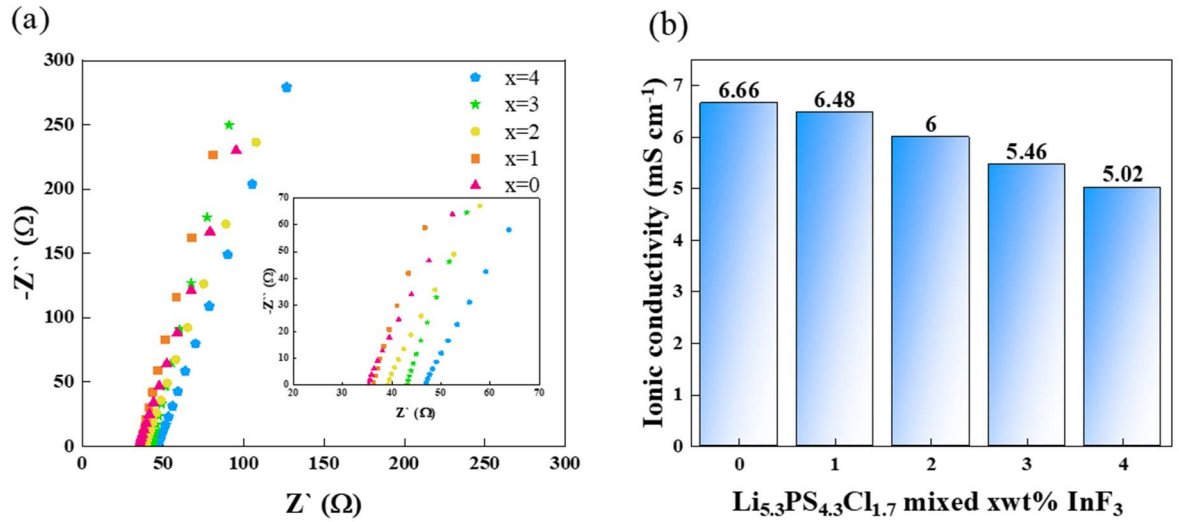

Figure 3.3. (a) Nyquist plots and (b) Ionic conductivity trend of $Li_{5.3}PS_{4.3}Cl_{1.7}$ mixed xwt% InF_3 (x = 0, 1, 2, 3, and 4) solid electrolytes at room temperature

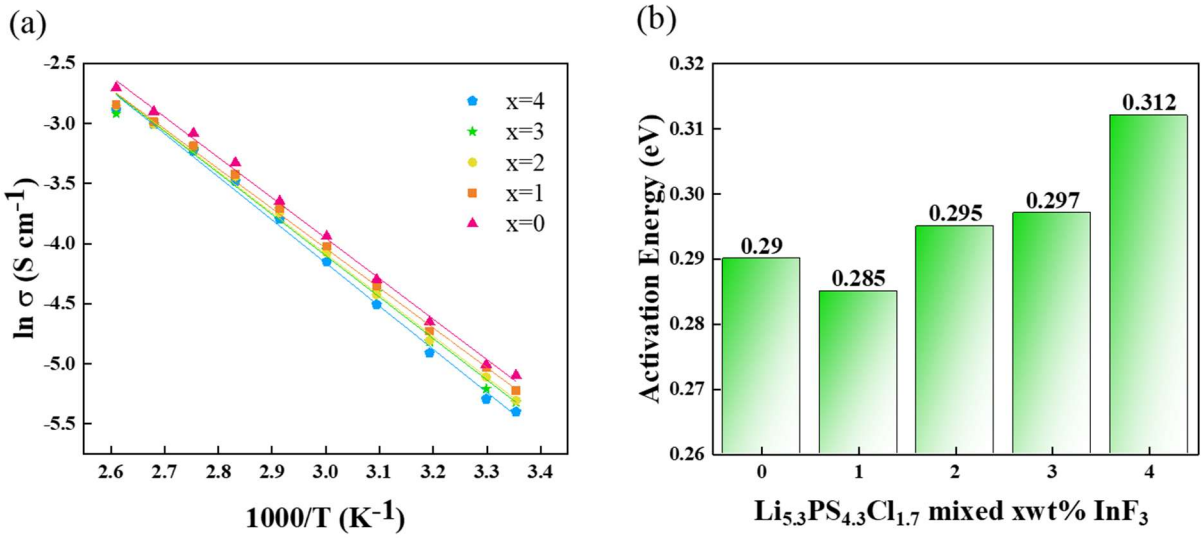

Figure 3.4. (a) Arrhenius ionic conductivity plots from 298K to 383K and (b) calculated activation energy trend of $Li_{5.3}PS_{4.3}Cl_{1.7}$ mixed xwt% InF_3 (x = 0, 1, 2, 3, and 4) solid electrolytes.

To evaluate the solid electrolyte's electrochemical stability window, cyclic voltammetry (CV) was performed. Figure 3.5 shows the CV data of the fabricated Li/SE/SUS asymmetric 2032 type coin cell.

For all compositions, the CV graph has a similar shape. As a result of investigating all samples from -0.5V to 5V (vs Li/Li^+), Peaks occurring due to lithium deposition ($Li^+ + e^- \rightarrow Li$) and dissolution ($Li \rightarrow Li^+ + e^-$) observe around -0.5V and 0.5V. Afterwards, it shows stable electrochemical stability without significant side reaction peaks up to the 5V range.

As mentioned in the previous section, Indium is a metal that easily forms an alloy with Lithium, and its redox potential occurs at 0.6V. In the case of the CV graph of pristine LPSCl, the lithium oxidation peak that occurs around 0.5V rises upward and then falls relatively quickly. However, when InF_3 is mixed in a solid electrolyte, especially in the case of x=3, the peak slowly falls to the 2V range. This is a peak that occurs when Li-In alloy forms.

When argyrodite-based solid electrolyte is in direct contact with lithium, the interfacial reaction proceeds slowly but clearly [21]. In the CV graph of pristine LPSCl, the curve is not smooth even after 1V, but the solid electrolyte mixed with InF_3 is smoother than pristine LPSCl. Additionally, as the mixing ratio of InF_3 increases, the intensity of the redox peak generated by lithium tends to increase. It is reasonable that mixing InF_3 into the solid electrolyte helps improve electrochemical performance at the interface with lithium.

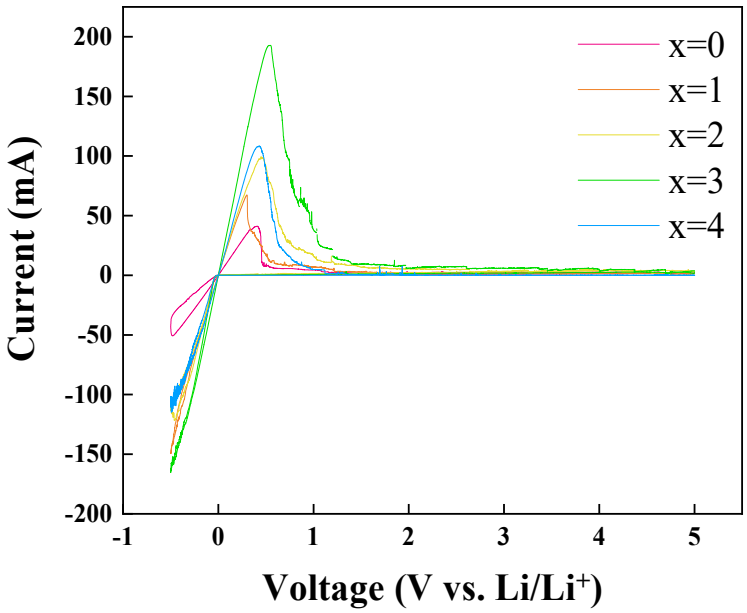

Figure 3.5. Cyclic voltammetry profiles of solid electrolytes at a scan rate of 1 mV/s at room temperature.

We believed that mixing InF_3 would cause the $3Li + InF_3 \rightarrow 3LiF + In$ reaction at the interface between the Li anode and the solid electrolyte during the charge and discharge process to form SEI containing LiF. Because LiF has low electronic conductivity, it can effectively inhibit Li dendrite growth. To investigate the electrochemical performance of solid electrolyte samples, we fabricate all ASSBs using the composite as the cathode and Li as the anode material. The cathode composite for ASSB is a mixture of cathode active material ($LiNbO_3$ coated NCM811), a conductive material (VGNF) and LPSCl. The initial charge-discharge curve and cycle stability of ASSB fabricated using $Li_{5.3}PS_{4.3}Cl_{1.7}$ mixed xwt% InF_3 (x = 0, 1, 2, 3, and 4) solid electrolyte are shown in Figure 3.6, and detailed cell performance values are given in Table 3.1. The ASSBs operate with a voltage range of 2.6-4.3V at 0.1c-rate.

In the case of pristine LPSCl, the initial discharge capacity determines 156.6mAh/g, the coulombic efficiency was 73.74%, and the capacity retention rate was 85.50% up to the 50th cycle. In all cases, the solid electrolyte mixed with InF_3 showed higher initial discharge capacity, coulombic efficiency, and capacity retention rate than pristine LPSCl. The greater the amount of InF_3 mixed up to 97LPSCl-3InF, the higher the retention rate and coulombic efficiency. 97LPSCl-3InF showed an initial discharge capacity of 172.8mAh/g, coulombic efficiency of 78.54%, and capacity retention rate of 93.58%, showing the highest coulombic efficiency and retention rate among all compositions. If charge movement occurs due to an unwanted side reaction at the interface between the electrode and the solid electrolyte in the first charge/discharge cycle, it can be expressed as an increase in charge capacity. In other words, the coulombic efficiency decreases. Therefore, it can be interpreted that the mixing of InF_3 contributes to reducing the degree of side reactions by covering the gap between the electrochemical stability window of the solid electrolyte and lihium metal, and we believe that LiF, which has a wide electrochemical stability window, would have played that role.

However, the performance of the 96LPSCl-4InF solid electrolyte decreased overall in all aspects, with an initial discharge capacity of 171.9mAh/g, coulombic efficiency of 77.64%, and capacity retention rate of 91.39%. This interface stabilizing effect is appropriate up to x=3, but has the opposite effect at x=4. 96LPSCl-4InF solid electrolyte has low ionic conductivity and high activation energy due to excessive InF_3. Mixing an appropriate amount of InF_3 into the solid electrolyte stabilizes the interface between Li metal and the solid electrolyte sufficiently to overcome the adverse effects of low ionic conductivity.

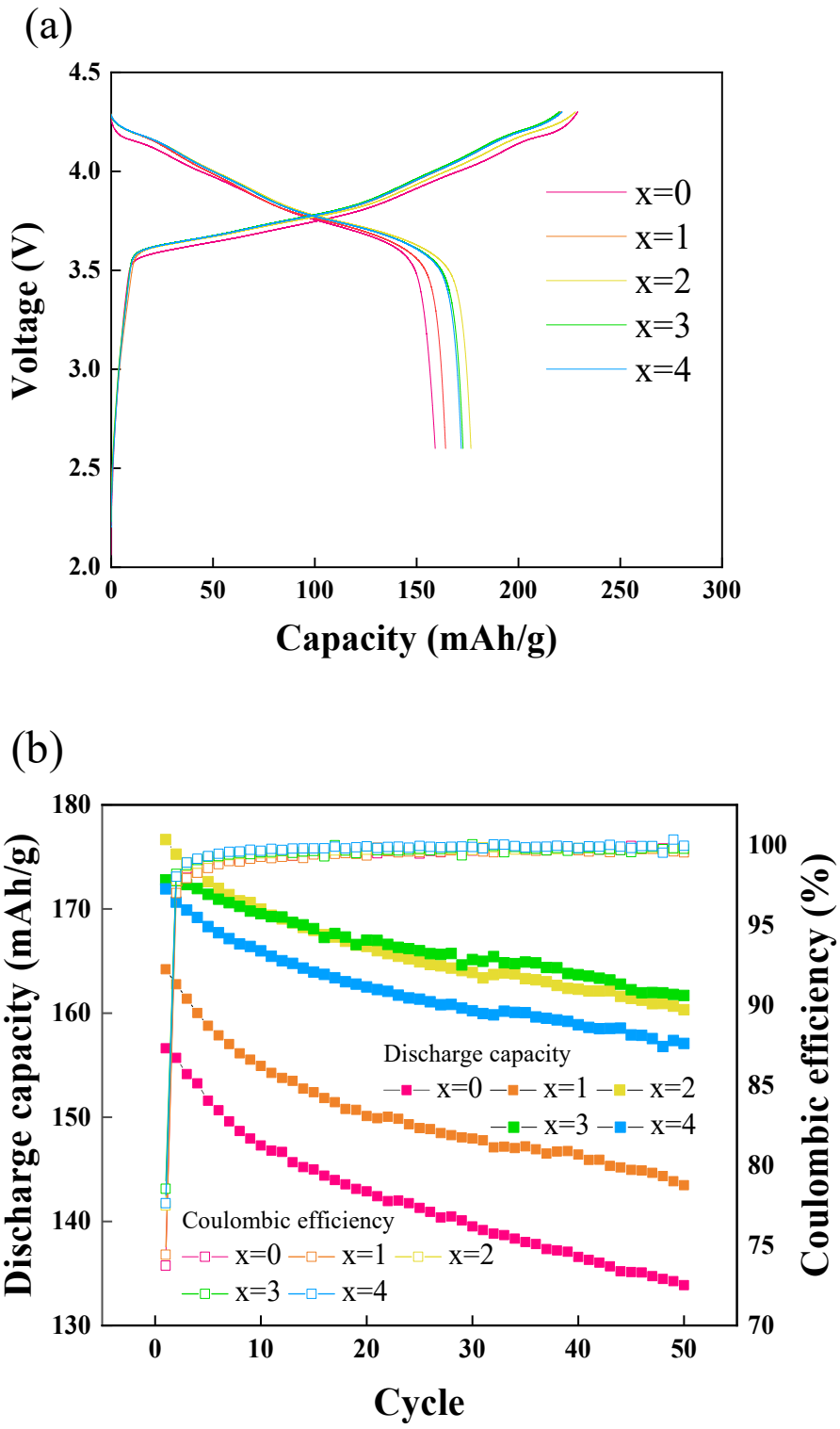

Figure 3.6. (a) First cycle of charge-discharge performance and (b) cycle stability of ASSBs fabricated using $Li_{5.3}PS_{4.3}Cl_{1.7}$ mixed xwt% InF_3 (x = 0, 1, 2, 3, and 4) solid electrolytes.

Table 3.1. Discharge capacity values, capacity retention, and coulombic efficiency of ASSBs fabricated using $Li_{5.3}PS_{4.3}Cl_{1.7}$ mixed xwt% InF_3 (x = 0, 1, 2, 3, and 4) solid electrolytes.

	X=0	X=1	X=2	X=3	X=4
1^{st} cycle Discharge capacity (mAh/g)	156.6	164.2	176.7	172.8	171.9
11^{th} cycle Discharge capacity (mAh/g)	146.8	154.3	169.4	169.3	165.5
21^{th} cycle Discharge capacity (mAh/g)	142.4	149.9	166.0	167.0	162.3
31^{th} cycle Discharge capacity (mAh/g)	139.2	147.8	163.4	165.0	160.0
41^{th} cycle Discharge capacity (mAh/g)	136.3	145.9	162.1	163.5	158.6
50^{th} cycle Discharge capacity (mAh/g)	133.9	143.5	160.3	161.7	157.1
1^{st} – 50^{th} cycle retention (%)	85.50	87.39	90.72	93.58	91.39
Coulombic efficiency in 1^{st} cycle (%)	73.74	74.42	77.49	78.54	77.64

3-4. Conclusion

An attempt was made to mix InF_3 with LPSCl solid electrolyte to reduce electrochemical instability between the Li metal anode and solid electrolyte and suppress lithium dentrite growth. LPSCl synthesis through high-energy ball milling and InF_3 was mixed by hand grinding. The 97LPSCl-3InF solid electrolyte showed an ionic conductivity of 5.46mS/cm at room temperature. The electrochemical stability of solid electrolytes toward lithium metal was studied using cyclic voltammetry. In the CV graph, 97LPSCl-3InF solid electrolyte has a lithium oxide peak with greater intensity than pristine LPSCl, and the peak size slowly decreases to the 2V range. This is an effect of the Li-In alloy formation peak occurring at 0.6V. Furthermore, the ASSB made with $LiNbO_3$ coated NCM811/97PSCl-3InF/Li showed a higher specific capacity of 172.8mAh/g than the ASSB made with $LiNbO_3$ coated NCM811/LPSCl/Li, and had an excellent retention rate of 93.58% until the 50th cycle. We believe that the highest coulombic efficiency of 78.54% shown by ASSB with 97LPSCl-3InF solid electrolyte is the result of suppressing side reactions occurring between the anode and solid electrolyte by forming LiF, which has a wide electrochemical stability window in the SEI.

3-5. References

[1] J. Lau, R.H. DeBlock, D.M. Butts, D.S. Ashby, C.S. Choi, B.S. Dunn, Sulfide solid electrolytes for lithium battery applications, Adv Energy Mater. 8 (2018) 1800933.

[2] M. Li, C. Wang, Z. Chen, K. Xu, J. Lu, New concepts in electrolytes, Chem Rev. 120 (2020) 6783–6819.

[3] F. Zheng, M. Kotobuki, S. Song, M.O. Lai, L. Lu, Review on solid electrolytes for all-solid-state lithium-ion batteries, J Power Sources. 389 (2018) 198–213.

[4] Y.-K. Sun, Promising all-solid-state batteries for future electric vehicles, ACS Energy Lett. 5 (2020) 3221–3223.

[5] J.-U. Cho, R. Rajagopal, D.H. Yoon, Y.J. Park, K.-S. Ryu, Control of side reactions using $LiNbO_3$ mixed/doped solid electrolyte for enhanced sulfide-based all-solid-state batteries, Chemical Engineering Journal. 452 (2023) 138955.

[6] A.M. Nolan, Y. Zhu, X. He, Q. Bai, Y. Mo, Computation-accelerated design of materials and interfaces for all-solid-state lithium-ion batteries, Joule. 2 (2018) 2016–2046.

[7] D. Cao, X. Sun, Q. Li, A. Natan, P. Xiang, H. Zhu, Lithium dendrite in all-solid-state batteries: growth mechanisms, suppression strategies, and characterizations, Matter. 3 (2020) 57–94.

[8] B. Li, Y. Chao, M. Li, Y. Xiao, R. Li, K. Yang, X. Cui, G. Xu, L. Li, C. Yang, Y. Yu, D.P. Wilkinson, J. Zhang, A review of solid electrolyte interphase (SEI) and dendrite formation in lithium batteries, Electrochemical Energy Reviews. 6 (2023) 7.

[9] C. Heubner, S. Maletti, H. Auer, J. Hüttl, K. Voigt, O. Lohrberg, K. Nikolowski, M. Partsch, A. Michaelis, From lithium-metal toward anode-free solid-state batteries: current developments, issues, and challenges, Adv Funct Mater. 31 (2021) 2106608.

[10] W.D. Richards, L.J. Miara, Y. Wang, J.C. Kim, G. Ceder, Interface stability in solid-state batteries, Chemistry of Materials. 28 (2016) 266–273.

[11] S. Wenzel, S.J. Sedlmaier, C. Dietrich, W.G. Zeier, J. Janek, Interfacial reactivity and interphase growth of argyrodite solid electrolytes at lithium metal electrodes, Solid State Ion. 318 (2018) 102–112.

[12] M. Nagao, A. Hayashi, M. Tatsumisago, Bulk-type lithium metal secondary battery with indium thin layer at interface between Li electrode and Li_2S-P_2S_5 solid electrolyte, Electrochemistry. 80 (2012) 734–736.

[13] A.L. Santhosha, L. Medenbach, J.R. Buchheim, P. Adelhelm, The indium− lithium electrode in solid-state lithium-ion batteries: phase formation, redox potentials, and interface stability, Batter Supercaps. 2 (2019) 524–529.

[14] Y. Zhu, X. He, Y. Mo, Origin of outstanding stability in the lithium solid electrolyte materials: insights from thermodynamic analyses based on first-principles calculations, ACS Appl Mater

Interfaces. 7 (2015) 23685–23693.

[15] R. Pathak, K. Chen, A. Gurung, K.M. Reza, B. Bahrami, J. Pokharel, A. Baniya, W. He, F. Wu, Y. Zhou, K. Xu, Q. Qiao, Fluorinated hybrid solid-electrolyte-interphase for dendrite-free lithium deposition, Nat Commun. 11 (2020) 93.

[16] Y. Yuan, F. Wu, Y. Bai, Y. Li, G. Chen, Z. Wang, C. Wu, Regulating Li deposition by constructing LiF-rich host for dendrite-free lithium metal anode, Energy Storage Mater. 16 (2019) 411–418.

[17] Y. Lu, Z. Tu, L.A. Archer, Stable lithium electrodeposition in liquid and nanoporous solid electrolytes, Nat Mater. 13 (2014) 961–969.

[18] W. Huang, L. Cheng, S. Hori, K. Suzuki, M. Yonemura, M. Hirayama, R. Kanno, Ionic conduction mechanism of a lithium superionic argyrodite in the Li–Al–Si–S–O system, Mater Adv. 1 (2020) 334–340.

[19] S. V Patel, S. Banerjee, H. Liu, P. Wang, P.-H. Chien, X. Feng, J. Liu, S.P. Ong, Y.-Y. Hu, Tunable Lithium-Ion Transport in Mixed-Halide Argyrodites $Li_{6-x}PS_{5-x}ClBr_x$: An Unusual Compositional Space, Chemistry of Materials. 33 (2021) 1435–1443.

[20] D.A. Ziolkowska, W. Arnold, T. Druffel, M. Sunkara, H. Wang, Rapid and economic synthesis of a Li_7PS_6 solid electrolyte from a liquid approach, ACS Appl Mater Interfaces. 11 (2019) 6015–6021.

[21] S. Wenzel, S.J. Sedlmaier, C. Dietrich, W.G. Zeier, J. Janek, Interfacial reactivity and interphase growth of argyrodite solid electrolytes at lithium metal electrodes, Solid State Ion. 318 (2018) 102–112.

Chapter 4. Summary

Two experiments were conducted with the purpose of improving the interfacial stability between the solid electrolyte and the anode and cathode electrodes.

First, in order to stabilize the interface between the solid electrolyte and the cathode, $LiTaO_3$ was simply mixed with LPSCl. When $LiTaO_3$ was mixed with LPSCl solid electrolyte, ionic conductivity slightly decreased. The 94LPSCl-6LTaO solid electrolyte showed an ionic conductivity of 5.32mS/cm at room temperature, but the critical current density in DC polarization technology was 0.65mA/cm^2, which was slightly higher than that of pristine LPSCl. ASSB made from non-coated NCM811/94LPSCl-6LTaO/Li achieved excellent cycle performance with higher specific capacity (174.4mAh/g) and retention rate of 74.4% than ASSB made from non-coated NCM811/LPSCl/Li. The ASSB fabricated from 94LPSCl-6LTaO mixed non-coated NCM811/94LPSCl-6LTaO/Li achieved a specific capacity of 177.3mAh/g and a higher retention rate of 76.3%. As a result of impedance analysis, when $LiTaO_3$ was simply mixed in both the solid electrolyte layer and the cathode composite, the resistance due to CEI was measured to be 1009.0Ω. This is a result of a decrease of about 64% compared to the case of not mixing $LiTaO_3$ at all, and a decrease of about 35% compared to the case of mixing $LiTaO_3$ only in the solid electrolyte layer. We conclude that these high specific capacity values and excellent cycling performance are due to the improved stability between the solid electrolyte and the cathode during the electrochemical reaction due to the simple mixing of $LiTaO_3$.

Second, InF_3 was simply mixed with LPSCl to stabilize the interface between the solid electrolyte and Li anode and suppress lithium dentrite growth. When InF_3 was mixed with LPSCl solid electrolyte, ionic conductivity decreased slightly. The 97LPSCl-3InF solid electrolyte showed an ionic conductivity of 5.46mS/cm at room temperature. In the Cyclic Voltammetry, the 97LPSCl-3InF solid electrolyte has a lithium oxide peak with greater intensity than the original LPSCl, and the peak size gradually decreases to the 2V range. This is an effect of the Li-In alloy formation peak occurring at 0.6V. Furthermore, the ASSB made with $LiNbO_3$ coated NCM811/97PSCl-3InF/Li showed a higher specific capacity of 172.8mAh/g than the ASSB made with $LiNbO_3$ coated NCM811/LPSCl/Li, and had an excellent retention rate of 93.58% until the 50th cycle. We believe that the highest coulombic

efficiency of 78.54% shown by ASSB with 97LPSCl-3InF solid electrolyte is the result of suppressing side reactions occurring between the anode and solid electrolyte by forming LiF, which has a wide electrochemical stability window in the SEI. Simple mixing of InF_3 can help stabilize the interface between Li anode and solid electrolyte.